AD-A186 158 ASSESSMENT OF VAS-DERIVED PRODUCTS CREATED BY A SIMULTANEOUS ALGORITHM ON.. (U) AIR FORCE INST OF TECH WRIGHT-PATTERSON AFB OH M J ANDREWS 1987 1/2

UNCLASSIFIED AFIT/CI/NR-87-104T F/G 4/2 NL

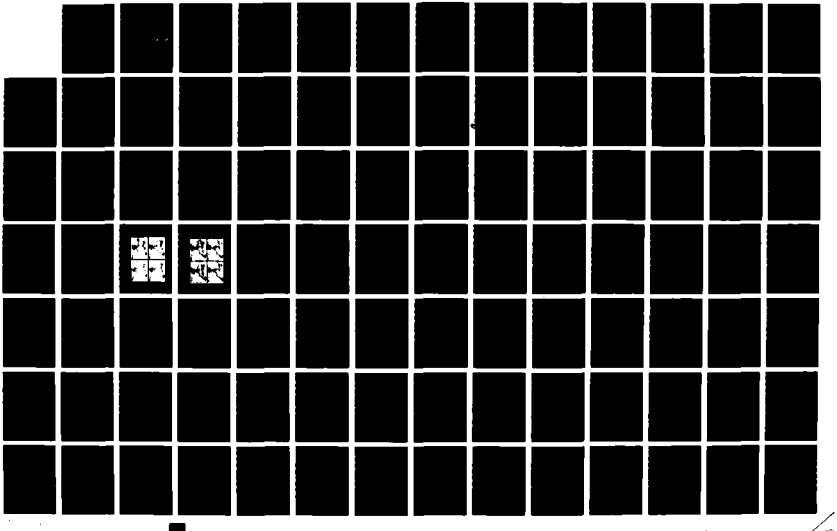

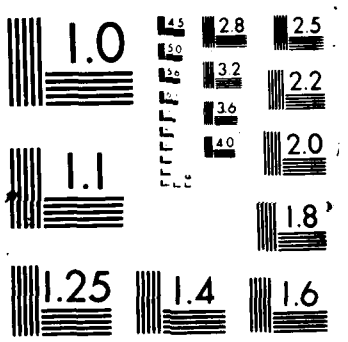
1.0
1.1
1.25
1.4
1.6
2.8
3.2
3.6
4.0
2.5
2.2
2.0
1.8

UNCLASSIFIED
SECURITY CLASSIFICATION OF THIS PAGE (When Data Entered)

# REPORT DOCUMENTATION PAGE

READ INSTRUCTIONS BEFORE COMPLETING FORM

1. REPORT NUMBER: AFIT/CI/NR 87-104T
2. GOVT ACCESSION NO.: /
3. RECIPIENT'S CATALOG NUMBER:

4. TITLE (and Subtitle): Assessment Of Vas-Derived Products Created By A Simultaneous Algorithm On A Convectively Active Day

5. TYPE OF REPORT & PERIOD COVERED: THESIS/DISSERTATION

6. PERFORMING ORG. REPORT NUMBER:

7. AUTHOR(s): Mark J. Andrews

8. CONTRACT OR GRANT NUMBER(s):

9. PERFORMING ORGANIZATION NAME AND ADDRESS: AFIT STUDENT AT: The Florida State University

10. PROGRAM ELEMENT, PROJECT, TASK AREA & WORK UNIT NUMBERS:

11. CONTROLLING OFFICE NAME AND ADDRESS: AFIT/NR, WPAFB OH 45433-6583

12. REPORT DATE: 1987

13. NUMBER OF PAGES: 109

14. MONITORING AGENCY NAME & ADDRESS (if different from Controlling Office):

15. SECURITY CLASS. (of this report): UNCLASSIFIED

15a. DECLASSIFICATION DOWNGRADING SCHEDULE:

16. DISTRIBUTION STATEMENT (of this Report)

APPROVED FOR PUBLIC RELEASE; DISTRIBUTION UNLIMITED



17. DISTRIBUTION STATEMENT (of the abstract entered in Block 20, if different from Report)

18. SUPPLEMENTARY NOTES: APPROVED FOR PUBLIC RELEASE: IAW AFR 190-1

LYNN E. WOLAVER 23 Oct 87
Dean for Research and Professional Development
AFIT/NR

19. KEY WORDS (Continue on reverse side if necessary and identify by block number)

20. ABSTRACT (Continue on reverse side if necessary and identify by block number)

ATTACHED

DD FORM 1 JAN 73 1473 EDITION OF 1 NOV 65 IS OBSOLETE

SECURITY CLASSIFICATION OF THIS PAGE (When Data Entered)

THE FLORIDA STATE UNIVERSITY

COLLEGE OF ARTS AND SCIENCES

# ASSESSMENT OF VAS-DERIVED PRODUCTS CREATED BY A SIMULTANEOUS ALGORITHM ON A CONVECTIVELY ACTIVE DAY

by

MARK J. ANDREWS

A Thesis submitted to the
Department of Meteorology
in partial fulfillment of the
requirements for the degree of
Master of Science



Approved:

Henry E. Fuelberg
Professor Directing Thesis

Ellen Thacker

Ronald W. Arritt

May 1987

## ABSTRACT

GOES-VAS satellite retrievals created by a new "simultaneous" algorithm are examined for a case in July 1982. The primary goals are to determine the spatial and temporal characteristics of the data, as well as the magnitudes of mean and RMS errors. Then, several integrated and non-integrated stability parameters are examined to assess VAS's capability for providing useful information in convective storms forecasting.

Results indicate that the new algorithm provides a much better estimate of moisture than the older "physical" variety. On the other hand, temperature showed no improvement.

The improved moisture information has a positive impact on various stability indices. A VAS-derived Lifted Index appears to be a promising convection forecast tool. Many small scale features in satellite imagery were related to the Lifted Index analyses. Also, the VAS-derived values provided information that could not be obtained from conventional surface data. The K Index and Total Totals Index also provided forecast data; however, their resolution did not appear as good as those of the

## ACKNOWLEDGEMENTS

I would like to thank Dr. Henry E. Fuelberg for his tireless assistance in preparing this thesis and translating my notes into readable English. Also, I would like to thank several others for their assistance: Dr. Eric Smith and Dr. David Stuart for reviewing this manuscript and providing insight into presenting the results, Gary Jedlovec for preparing the simultaneous VAS profiles for this case, Dr. Christopher Hayden for answering short-notice questions about the retrieval algorithms, Dr. James Purdom for supplying the integrated-index software, the United States Air Force for supporting my education at Florida State, and finally Dina, my fiance, for proofing the manuscript and her patience in many word-processing weekends. The National Aeronautics and Space Admininstration provided research support through Contract NAG8-033 under the auspices of the Atmospheric Physics Branch of the Marshall Space Flight Center.

TABLE OF CONTENTS

## LIST OF TABLES

## LIST OF FIGURES

LIST OF FIGURES (CONTINUED)

LIST OF FIGURES (CONTINUED)

LIST OF FIGURES (CONTINUED)

## 1. Introduction

With the launch of the first Visible Infrared Spin-Scan Radiometer (VISSR) Atmospheric Sounder (VAS) onboard a geostationary platform in the fall of 1980, forecasters have had a significant increase in the amount of data available for the analysis and prognostication of both large and small scale weather phenomena such as severe storms and mid-latitude cyclones. The 12 VAS channels measure infrared radiation in bands from 3.5 to 15 μm. Their information can be used in a variety of ways. For example, channel imagery can be used independently, such as done with the 6.7 μm water vapor band which is used to observe mid-tropospheric humidity (e.g., Petersen *et al.*, 1982). Other applications of 6.7 μm imagery include the generation of horizontally enhanced fields of middle level mixing ratios (e.g., Steranka *et al.*, 1973), wind determination by tracking vapor features (e.g., Stewart *et al.*, 1985), and inferring the characteristics of upper level jet streams and jet streaks (e.g., Rodgers *et al.*, 1976; Raymond *et al.*, 1981; Stewart and Fuelberg, 1986). For deriving vapor content nearer the surface, Chesters *et al.* (1983) used the "split window" technique, a combination of VAS channels 7 and 8. When employed with

channel information describing other levels of the atmosphere, areas of convective instability (dry mid-level air over moist low-level air) could be calculated (Petersen *et al.*, 1984).

If measurements from all VAS channels are utilized, the radiances can be transformed into vertical temperature and moisture profiles based on knowledge of the associated vertical weighting functions. There are currently two different approaches for creating these soundings. One method requires the development of statistical relationships between measured channel radiances at radiosonde locations and the actual radiosonde measurements. These regression equations then are used to calculate atmospheric parameters at the various levels of different sites. Conventional surface data also are frequently used in the equations (Lee *et al.*, 1983). Studies using the "statistical" retrievals demonstrated reasonable agreement with soundings from a special mesoscale radiosonde network, especially in the lower troposphere (Chesters *et al.*, 1984). The ability of statistical retrievals to describe the atmosphere's current moisture content has been examined extensively. For example, investigators have noted that they can provide valuable information about the pre-convective environment (Petersen *et al.*, 1984). Petersen *et al.* (1982) demonstrated that VAS stability calculations

provided valuable information between radiosonde data points, whereas Mostek *et al*. (1986) noted that regression-derived stability parameters exhibited accurate mesoscale resolution and continuity.

The second method of retrieval calculation involves inverting the radiative transfer equation. This "physical" algorithm (Smith, 1983) uses an iterative convergence scheme to determine the sounding profile which fits the measured channel radiances with the least amount of residual error. The iterations loop between the temperature and dewpoint profile, making each dependent upon the other. A study of mesoscale air masses based on these physical retrievals (Zehr, 1985) suggested that VAS information could provide mesoscale convection forecasts. Leftwich (1985) found hail forecasts using VAS profiles were timelier and more accurate than radiosonde generated profiles. Operational use of physical retrievals at the National Severe Storms Forecast Center (NSSFC) has been documented by Anthony and Wade (1983). One unfortunate aspect of VAS physical profiles is a large 2 - 4°C diurnal temperature variation extending well above the boundary layer (Fuelberg and Funk, 1987).

Investigations into the accuracy of the two VAS retrieval methods have been conducted by several researchers. Comparisons with radiosonde-derived "ground truth" data (Jedlovec, 1985) have indicated bias errors

less than 4 °C for temperature and 3-6.5 °C for dewpoint profiles in the case of physical retrievals. Errors less than 3.5°C (temperature) and less than 2 °C (dewpoint) were associated with the regression algorithm. Physical temperature retrievals had slightly smaller Root Mean Square (RMS) errors (1.7°C) than the regression retrievals (2.0°C). In contrast, however, the regression dewpoint profiles had smaller RMS errors (4.8°C) than the physical retrievals (5.9°C). Results of both algorithms also have been evaluated using statistical structure functions (Fuelberg and Meyer, 1985). Random errors in the VAS profiles were comparable to those from radiosondes, with the physical algorithm showing slightly better results. Similarly, horizontal gradients from the physically derived soundings were more meaningful than those from the statistical approach.

A new physical retrieval algorithm (Smith *et al.*, 1986; Smith and Woolf, 1984) has been devised to correct some of the documented problems of the original physical formulation (Smith, 1983), especially the large errors in moisture content. This new method uses a simultaneous solution system rather than an iterative scheme. Temperature and moisture calculations are made simultaneously, rather than being dependent upon each other. Thus far, only a few studies have utilized soundings from this recent approach. Wade *et al.* (1985)

presented several thermodynamic parameters generated in near real time for the NSSFC during May 1985. Kitzmiller (1986) tested well known stability indexes generated from VAS retrievals and found some predictor combinations to be promising for severe storm forecasting.

The purpose of this paper is to examine temperature and dewpoint profiles created by the new simultaneous algorithm for a period in July 1982. Although this case was previously documented by Fuelberg and Funk (1987) using the Smith (1983) physical retrieval algorithm, the current emphasis differs greatly from theirs. Specifically, the accuracy of temperature and dewpoint data will be statistically compared to radiosonde observations and to the older physical values used by Funk (1985). In addition, spatial and time continuities of the data fields generated by VAS will be examined. After discussing the apparent strengths and weaknesses of the new algorithm, numerous traditional parameters for thunderstorm forecasting will be examined. That section will focus on the following questions. Did VAS retrievals provide useful temporal or spatial information which was not available from the radiosonde observations (RAOBs)? What was the influence of the hourly surface data in generating the low level VAS temperature and moisture profiles; that is, did VAS provide information not contained in the hourly surface data?

It is important for the user of VAS data to understand strengths and weaknesses of the current satellite retrieval system. The intent of this paper is to help shed additional light on those products.

## 2. VAS Instrument

The VAS instrument is a passive radiometer capable of making simultaneous visible and infrared images of radiation upwelling from clouds, the earth's surface, and it's atmosphere. VAS is carried onboard the latest series of geostationary spacecraft (GOES). Compared to polar orbiting platforms, the geostationary configuration permits a much faster sampling rate for observing particular surface locations. The instrument spins at 100 rpm from west to east and steps a scan mirror from (usually) north to south. The reader is referred to Menzel *et al.* (1981) for a detailed description of the VAS instrument and its operational modes. Briefly stated, however, VAS consists of 8 visible channel detectors and 6 thermal detectors, the latter measuring infrared radiation in 12 channels with central wavelengths ranging from 3.7 to 15 μm (See Table 1, Fig. 1). Fields of View (FOV) of the visible detectors possess a 1 km resolution at satellite nadir, while the thermal detectors have a 7 or 14 km resolution depending on the type being employed. A filter wheel placed in front of the detectors selects the spectral channel being used at the given moment.

Seven of the 12 spectral channels (Table 1, Fig.1) are

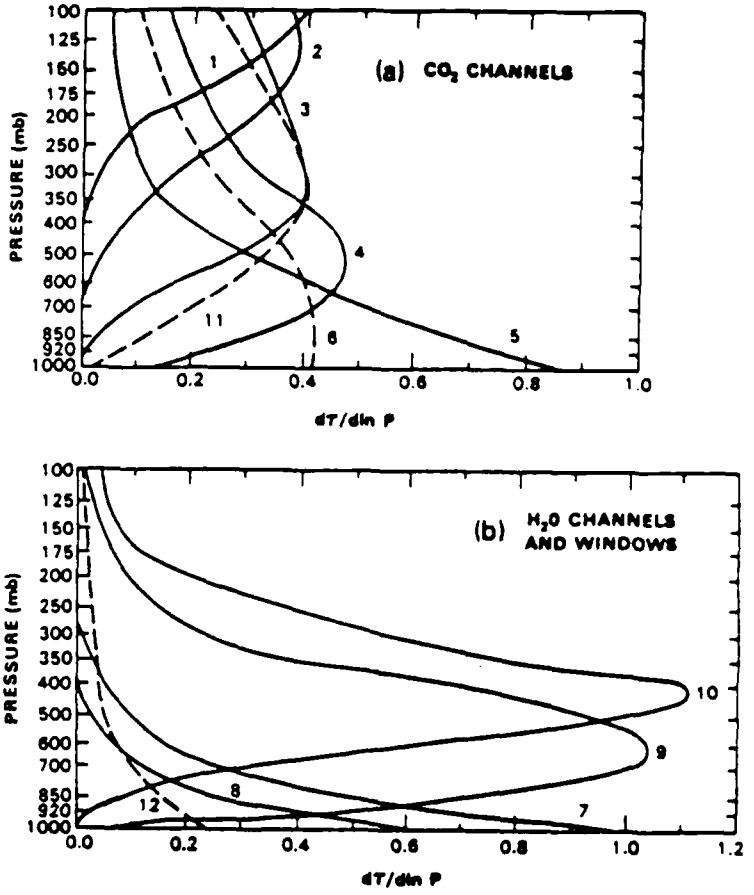


Fig. 1. HIRAS weighting functions, calculated from line-by-line molecular absorption coefficients for nadir view of the U.S. Standard Atmosphere in the (a) temperature sounding channels and (b) water vapor and window channels. Dashed lines indicate the shortwave channels (6, 11, and 12), which can be affected by reflected sunlight (after Chesters et al., 1983).

Table 1. VAS instrument characteristics (after Smith,1983).

| Spectral channel | Central wavelength (μm) | Weighting function peak (mb) | Absorbing constituent | Typical DS spin budget |
|---|---|---|---|---|
| 1 | 14.7 | 40 | $CO_2$ | 2 |
| 2 | 14.5 | 70 | $CO_2$ | 4 |
| 3 | 14.2 | 150 | $CO_2$ | 7 |
| 4 | 14.0 | 450 | $CO_2$ | 7 |
| 5 | 13.3 | 950 | $CO_2$ | 4 |
| 6 | 4.5 | 850 | $CO_2$ | 7 |
| 7 | 12.7 | surface | $H_2O$ | 3 |
| 8 | 11.2 | surface | window | 1 |
| 9 | 7.2 | 600 | $H_2O$ | 9 |
| 10 | 6.7 | 400 | $H_2O$ | 2 |
| 11 | 4.4 | 500 | $CO_2$ | 7 |
| 12 | 3.9 | surface | window | 1 |

thermal $CO_2$ channels (1-6 and 11) whose radiance measurements can provide vertical temperature profiles. On the other hand, there are only 3 channels (7, 9 and 10) which yield moisture data. Finally, channels 8 and 12 give surface or cloud top information.

Knowledge of the absorption characteristics of several atmospheric constituents ($CO_2$, $N_2$, $N_2O$, NO, $CH_4$, $O_2$, and $H_2O$) gives the weighting functions, $d\tau/d \ln p$ of the 12 spectral channels displayed in Fig. 1. Although each channel detects radiation over a considerable atmospheric depth, peaks for the moisture channels are relatively sharp, due to the rapid decrease of water vapor with altitude in the lower troposphere. Even though each channel peaks at a different level, the weighting functions have considerable overlap, contributing to VAS's poor vertical resolution.

VAS has 3 operating modes, the Dwell Sounding (DS) mode, the Multi-Spectral Imaging (MSI) mode, and the Dwell Imaging (DI) mode. Each can use any of the visible and infrared channels. Capable of receiving instructions from the ground, the instrument can scan any subset of the earth's disk, with scanning time dependent upon mode selection and size of the observed area.

The DS mode was designed to improve signal to noise ratios of the radiance measurements so that sounding profiles can be retrieved. This is achieved by keeping the

scanning mirror fixed on a given line for a predetermined number of instrument revolutions for each spectral channel programmed. Thus, the multiple passes over the same locations provide an averaging process that partially filters random error in the data. The number of spins per line varies with channel and is called the spin budget (Table 1). In addition, a spatial averaging of several horizontal fields of view also is used to improve signal to noise ratios. Of course, this decreases the horizontal sounding resolution, often down to near 75 km. Due to multiple passes along each scanning line, operational time constraints do not permit the entire disk to be observed in this mode. About 30 minutes is required to observe 20 degrees of latitude (Petersen *et al.*, 1982).

The MSI mode permits larger areal coverage and more rapid rescanning since only a limited number of channels is sampled during a particular scan pass, i.e., up to 4 spectral bands, always including the visible channel. In the MSI mode the earth's disk can be observed every 30 minutes. Sounding retrievals are not prepared from MSI data.

The Dwell Imaging (DI) mode was created as a compromise between the DS and MSI configurations. Specifically, measurements are taken over all 12 channels; however, the spin budget is smaller than for the DS mode. Nonetheless, sounding retrieval still is performed although results are

considered not as reliable as those from the expanded budget. The DI mode permits coverage of the North American continent at 30 minute intervals (Smith *et al.*, 1982).

During severe storm situations, VAS measurements are pre-empted by Rapid Interval Scan Operations (RISOP) that provide more frequent visible and infrared window channel (8) imagery. Thus, retrieval products often are not prepared during severe weather events. This has limited many investigators to exploring VAS capabilities during pre-convective and non-severe weather cases.

## 3. Physical retrieval algorithms

### a. Original version

The physical retrieval algorithm involves the conversion of measured spectral radiances into vertical profiles of temperature and moisture by using the radiative transfer equation. More specifically, least squares analytical solution to the equation transforms a smooth "first guess" profile into an enhanced final version. Since a detailed discussion of this algorithm is presented by Smith (1983) only a summary follows.

The radiative transfer equation is of the form

$$R(\nu,\theta) = B(\nu,T_s)\,\tau(\nu,p_s,\theta) - \int_0^{p_s} B(\nu,T)\,\frac{\partial \tau(\nu,p,\theta)}{\partial \ln p}\,\frac{dp}{p}, \qquad (1)$$

where R is defined as the mean spectral radiance for wavenumber $\nu$ and local zenith angle $\theta$. B is the "Planck" radiance associated with temperature T, $\tau$ is the transmittance of the atmosphere above level p, and the subscript s denotes the opaque surface of the radiating atmosphere, either ground or cloud. Both B and $\tau$ are weighted with respect to the spectral response of the

particular channel. The model treats B and $\tau$ as monochromatic functions, thereby simplifying the computations.

Input data are assumed to be measurements of $R(\nu,\theta)$, a transmittance model providing $\tau$ functions, and estimates of $p_s$. A "first guess" temperature profile is required and can be constructed in a variety of ways. For example, climatology tables can be used to specify a standard atmosphere for a given latitude and season. Alternatively, a numerical analysis or forecast (12 h) from the NMC models can be employed, or previous VAS profiles can serve as the "guess" for the next profiles. In addition, observed surface data can (and usually) are blended with these starter profiles. Since the surface (cloud or ground) is assumed to be opaque, a subroutine is included to insure this requirement.

A "guess" mixing ratio profile is created from the first guess temperature sounding by assuming 50% relative humidity (RH) and then using the derivation of Smith and Zhou (1982)

$$RH = RH_o \exp \frac{R(\nu,\theta) - R(\nu, RH_o, \theta)}{\int_0^{p_s} Q(\nu, P, \theta)\, dp}, \qquad (2)$$

where $R(\nu,\theta)$ is the observed radiance corresponding to

the true distribution of precipitable water, $R(\nu, RH_o, \theta)$ is a radiance calculated for an assumed distribution of relative humidity $RH_o$, and $Q(\nu,p,\theta)$ is a moisture weighting function. Mean relative humidities are calculated for three layers bounded by 800, 600, and 300 mb, i.e., the approximate levels of weighting function peaks for the three VAS water vapor channels (7, 9, 10). If available, values of surface relative humidity also are utilized, otherwise the channel 7 derived RH value is used. A "smooth" water vapor profile is achieved by linearly interpolating between these calculated values. This step assumes a constant RH within the layer contributing radiation to each water vapor channel.

Once the guess profiles are prepared as described above, transmittance functions are calculated for the VAS thermal ($CO_2$) channels (1, 2, 3, 4, 5, 6, 11). Thermal channel radiances then are estimated by using (1) and (2) from the "guess" temperature and smooth moisture profiles. Following Smith (1983), differences between the measured brightness temperature $T_B(\nu)$ and $T_B^N(\nu)$, the brightness temperature which would be measured if the true temperature profile $T(p)$ equalled the estimate $T^N(p)$ can be expressed as

$$T_B(\nu) - T_B^N(\nu) = \int [T(p)-T^N(p)]W^N(\nu,p,\theta)\, dp/p, \qquad (3)$$

where N denotes the iteration step and $W^N(\nu,p,\theta)$ is the temperature profile weighting function. After normalizing the weighting function with respect to the expected error of the brightness temperatures, $W^*(\nu,p,\theta)$, an iterative solution of (3), proposed by Smith (1970) is used:

$$T^{n+1}(p) = T^n(p) + \sum_j \frac{W^*(\nu,p,\theta)[T_B(\nu)-T_B{}^N(\nu)]}{W^*(\nu,p,\theta)}, \qquad (4)$$

where j is the spectral channel index.

After the initial "guess" profile has been modified by (4), a new set of $CO_2$ channel radiances is calculated in a similar manner. Then, a convergence test is applied to determine whether the new temperature profile is significantly different, i.e., the change in brightness temperatures is compared to the "expected" error. When the change is less than an empirically derived noise factor, the new profile is determined to be the final version. If the profile fails the test, additional iterations are performed until convergence is achieved.

The iterative scheme unfortunately produces a smooth temperature profile. To partially rectify this problem, an enhancement procedure involving least squares solutions is applied. Specifically, it is assumed that the difference between the true profile T(p) and the retrieved profile $T^N(p)$ can be approximated by line segments expressed by three unknown quantities $dT_1$, $dT_2$, and $dT_3$ as shown in

Fig. 2. Similarly, the water vapor profile is enhanced by using a line segment approximation to the differences between the true and retrieved profiles.

Based on the above mentioned procedure, an enhanced water vapor profile is constructed and used in the transmittance model to calculate new, updated $CO_2$ transmittance functions. Then, a new enhanced temperature profile is calculated as in Fig. 2. Next an enhanced water vapor profile is computed again. Finally, dewpoints are obtained from the final moisture values.

b. Simultaneous algorithm

The "new" physical retrieval algorithm employs a different procedure for solving the radiative transfer equation (Smith *et al.*, 1986; Smith and Woolf, 1984). Instead of an iterative solution for the profiles, a simultaneous retrieval of temperature and moisture is performed. As in the original method described above, a "first guess" profile is required, and options available for its construction are similar. Only highlights of the algorithm are presented below.

In perturbation form, the radiative transfer equation can be expressed as

$$\delta R \cong \int_0^{P_s} \delta\tau \, dB + \int_0^{P_s} \tau \, d(\delta B), \qquad (5)$$

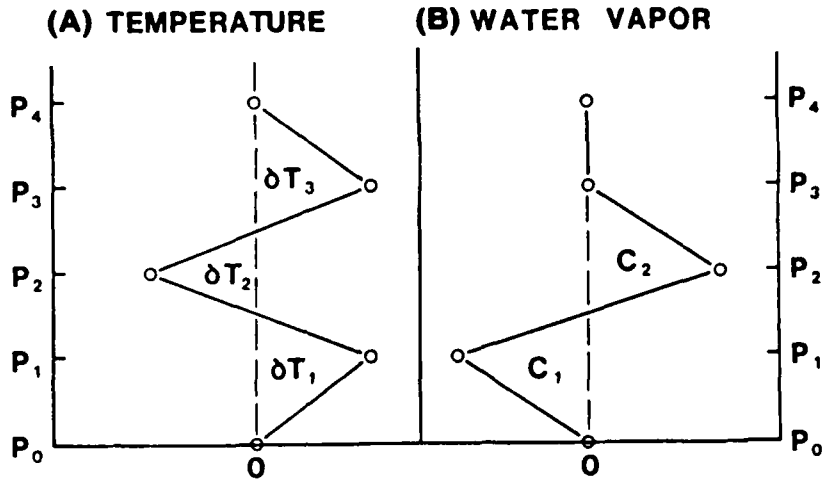


Fig. 2. Illustration of the line segment approximations used to model the fine-scale structure deviations of (a) atmospheric temperature and (b) water vapor from their vertically smoothed estimate (after Smith, 1983).

where dependency on angle, pressure, and frequency are eliminated for simplicity. The perturbations ($\delta$) are with respect to an a-priori condition (e.g., a "first guess" profile). Smith *et al.* (1986) assumed that the transmittance perturbation is dependent only on the uncertainty in the column of precipitable water (U). Integration of (5) and application of the assumption produce:

$$\delta T^* = \int_0^{P_s} \delta U \frac{\partial T}{\partial p} \frac{\partial \tau}{\partial U} \frac{(\partial B/\partial T)}{(\partial B/\partial T^*)} dp - \int_0^{P_s} \delta T \frac{\partial \tau}{\partial p} \frac{(\partial B/\partial T)}{(\partial B/\partial T^*)} dp + \delta T_s \frac{(\partial B_s/\partial T_s)}{(\partial B/\partial T^*)} \tau_{s}, \quad (6)$$

where $T^*$ is the brightness temperature, T is temperature, and $T_s$ is the surface skin temperature.

To solve for the perturbations from a set of spectrally independent radiance observations, arbitrary pressure functions $\phi(p)$ are used for $\delta T_s$, $\delta U(p)$, and $\delta T(p)$ in (6). Smith *et al.* (1986) selected the profile weighting functions ($d\tau/d \ln p$) of the radiative transfer equation as pressure basis functions. Substituting these functions into (6) yields a spectral radiance observation, $\delta T_j$, for the set of K channels:

$$\delta T_j^* = \sum_i \alpha_i \Phi_{ij}, \quad (7)$$

$$\text{where} \quad \Phi_{o,j} = \frac{\partial B_j / \partial T_s}{\partial B_j / \partial T_j^*} \tau_{s,j}$$

$$\Phi_{i,j} = \int_o^{P_s} \left[ \int_o^P g \phi_i \, dp \right] \left[ \frac{\partial T}{\partial p} \frac{\partial \tau_j}{\partial U} \frac{\partial B_j / \partial T}{\partial B_j / \partial T_j^*} \right] dp \qquad i \leq N$$

$$\Phi_{i,j} = \int_o^{P_s} \phi_i \left[ \frac{\partial \tau_j}{\partial p} \frac{\partial B_j / \partial T}{\partial B_j / \partial T_j^*} \right] dp. \qquad N < i \leq M \tag{8}$$

Other quantities needed to calculate the $\bar{\Phi}$ matrix are estimated from the first guess sounding. The exception is $d\tau/dU$ which is obtained from a mixing ratio profile with values at each level being half those of the first guess profile.

In matrix form (7) becomes

$$t^* = \Phi \alpha , \tag{9}$$

where $t^*$ is a row vector of K brightness temperature observations, $\alpha$ is a row vector of M+1 coefficients, and $\Phi$ is a matrix having dimensions (KxM+1). A least squares solution of (9) gives

$$\alpha = (\Phi^T \Phi + \gamma I)^{-1} \Phi^T t^* \tag{10}$$

where $(\ )^T$ denotes matrix transposition, $(\ )^{-1}$ indicates matrix inversion, and $\gamma$ is a scaler (usually 0.1)

multiplied by the identity matrix I and added to the $\mathbf{F}^T\mathbf{F}$ matrix in order to stabilize the matrix inverse. After the $\alpha$'s are determined, $\delta T_s$, $\delta q$, and $\delta T$ are known (by knowledge of the original basis functions). These values then are added to the first guess sounding to achieve a final profile.

There are two passes through the retrieval algorithm. The first uses only selected channels which are determined to be free of any cloud contamination. Then, a second pass is run using all available channels not considered to be seriously contaminated by clouds. The determination of channel contamination is discussed in detail by Smith *et al.* (1986).

There are several differences between the "old" and "new" versions of the physical algorithm. The "new" algorithm solves for temperature and water vapor concurrently, whereas the two parameters are calculated separately of each other in the "old" scheme. Consequently, any error in one parameter would be carried over to the other in the Smith (1983) procedure. Smith *et al.* (1986) noted that the simultaneous solution "alleviates the problem of the interdependence of the radiation observation upon the three parameters" (temperature, water vapor, and surface skin temperature). Another significant difference concerns the initial water vapor profiles used by the algorithms. The "new" version

utilizes a first guess profile rather than a 50% RH assumption based on the initial temperature sounding. Since a first guess water vapor profile should be superior to a crude 50% RH approximation, improved water vapor values would be expected from the "new" algorithm.

Documentation for the simultaneous algorithm is limited; however, Dr. C. M. Hayden of NESDIS (personal communication, 1987) noted that it should produce little change in temperature performance. On the other hand, considerable improvement is expected in humidity.

Even with advancements in the retrieval process over the past few years, there are still many possible sources of error in the "flow chart" from the beginning step of measuring radiation from the space platform itself to the final output of temperature and dewpoint. For example, one must consider the biases and noise of the radiometer. Also, the VAS instrument is a volume sensor, not providing a point source measure as done by radiosondes. Specifically, VAS has poor vertical resolution because of the inability to use spectral wavelengths which have high vertical resolution weighting functions (Fig. 1). Similarly, radiance measurements are representative of a horizontal area as well. Finally, one must consider the retrieval algorithm itself. Truncation errors introduced by the mathematics of matrix inversion and the introduction of a "first guess" profile are additional

concerns of which the forecaster must be aware. With the above mentioned limitations in mind, an examination of a case in July 1982 is presented.

## 4. Data

Since one of the goals was to investigate changes in performance between results of the "new" and "old" physical algorithms, the case studied by Fuelberg and Funk (1987) was chosen. Consequently, sounding times and areal coverage were similar to those of their research. VAS soundings were available over the central United States at 5 times: 1300, 1600, 1700, 2000, and 2300 GMT 21 July 1982. The satellite operated in the DI mode for the 1300 and 1600 GMT measurements, but in the DS mode for the latter 3 times.

VAS retrievals were prepared at the University of Wisconsin on the Man-computer Interactive Data Access System (McIDAS) (Smith *et al.*, 1979). An NMC 12 h forecast valid at 1200 GMT was used as the "first guess" profile for the 1300 GMT retrieval run. Thereafter, previous VAS profiles were employed. Retrieval data were available at 950 mb as well as the "mandatory" levels of the radiosonde code, i.e., the surface, and 850, 700, 500, 300, 250, 200, 150, and 100 mb.

McIDAS was used to edit any profiles contaminated by clouds or inconsistent with surrounding data. Then, after delivery to Florida State University, another editing

check was performed. Several deletions were done subjectively by the author, based on obvious data inconsistencies. Overall, the amount of editing was small, as only a few retrievals were eliminated. The number of soundings available after editing is given in Table 2 for each time. The midwestern United States was the area of interest, and data coverage there was excellent with only a few data gaps due to cloud cover being evident (Fig. 3). The average spacing for the retrievals was 125 km.

Radiosonde data for 1200 GMT 21 July and 0000 GMT 22 July 1982 were obtained from the National Climatic Center. Copies of NMC facsimile charts were gathered from local archives.

Table 2. Number of soundings within the computational domain after editing.

| Sounding Time (GMT) | Number of soundings |
|---|---|
| 1300 | 119 |
| 1600 | 127 |
| 1700 | 113 |
| 2000 | 122 |
| 2300 | 118 |

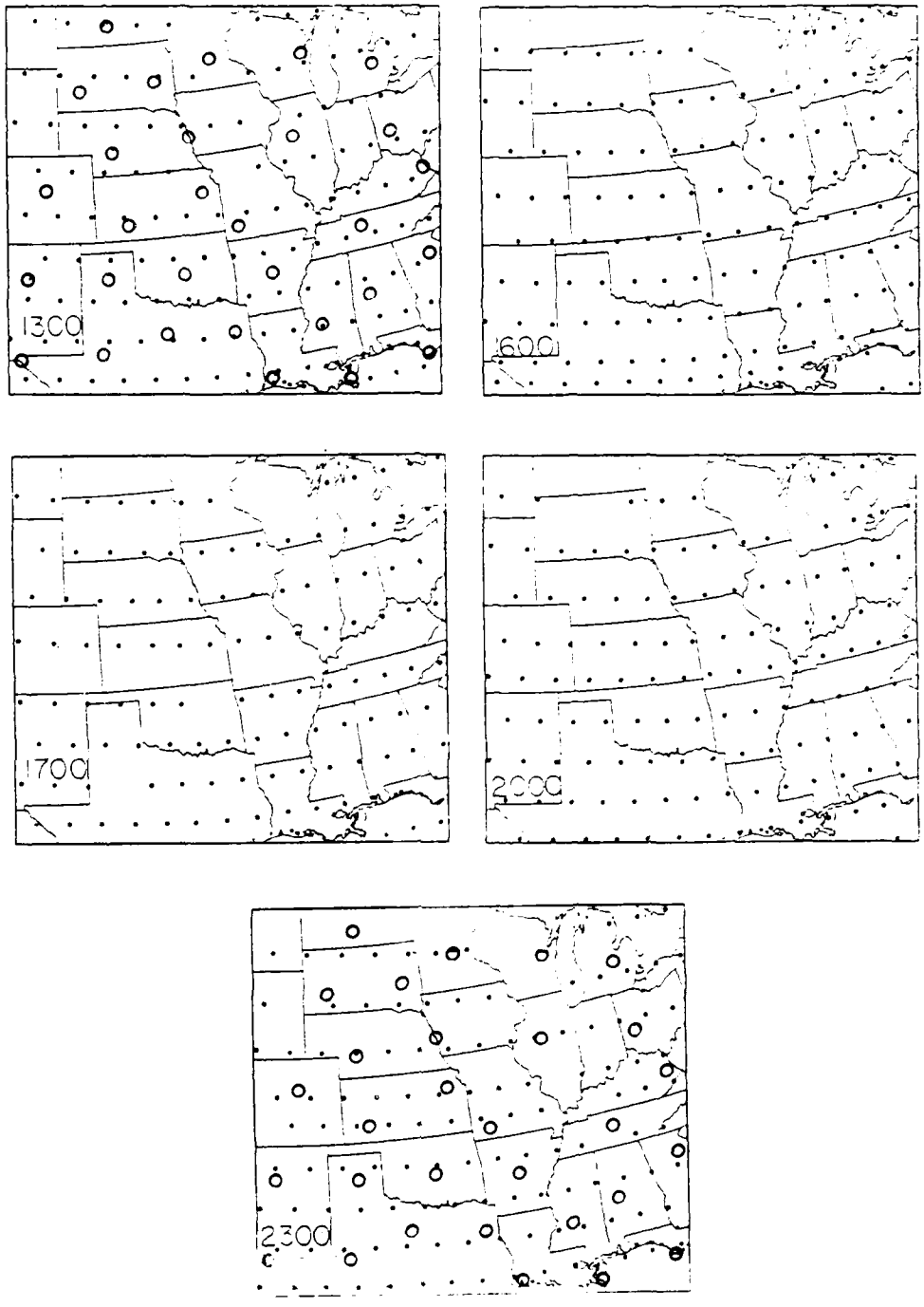


**Fig. 3.** Locations of edited VAS retrievals at observation times. Open circles the 1300 and 2300 GMT analyses repres the locations of available RAOBs at 1... GMT 21 July and 0000 GMT 22 J... respectively.

## 5. Synoptic conditions

Conditions on 21 July 1982 began much like those of the previous few days. The main baroclinic zone stretched along the northern border of the United States, while upper level dynamics elsewhere were weak.

The 1200 GMT NMC surface chart (Fig. 4) depicted a weak stationary front extending from a low pressure area over eastern Colorado through central Missouri and northern Georgia. Another cold front reached from northeastern Minnesota to northern Nebraska and central Montana, with a slightly cooler and drier airmass from Canada to its north. Skies over several areas contained remnants of nighttime convection (not shown). Showers and thunderstorms had persisted through the night over most of Minnesota, the eastern half of Nebraska, and northern Missouri. In addition, scattered thunderstorms were in progress over most of the Gulf Coast. Fog was evident over most of West Virginia, eastern Kentucky, and northern Louisiana. No apparent cloud features were associated with the front from Nebraska into Montana. Infrared imagery (not shown) indicated high level clouds covering South Carolina and Georgia, most likely debris from convection of the previous night.

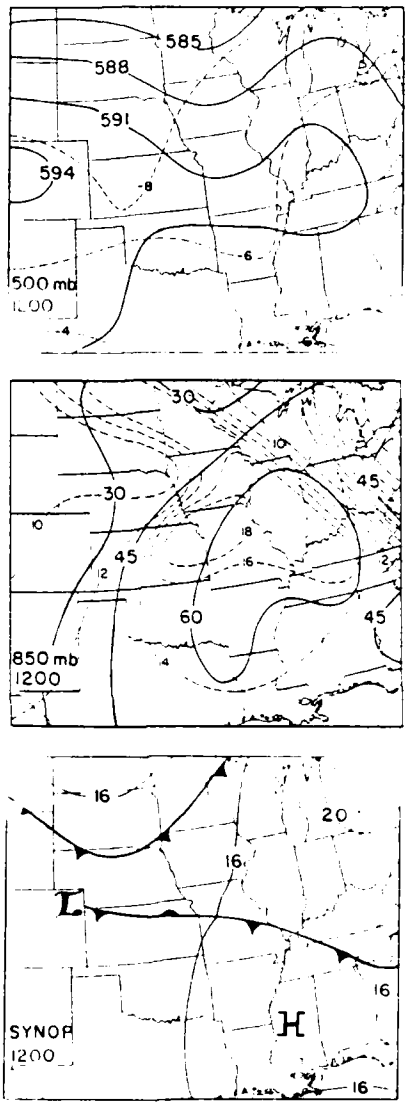


Fig. 4. Analyses at 1200 GMT 21 July 1982. At the surface, isobars are labeled in the usual convention. At 850 mb, heights are solid where 45 represents 1450 m, and isodrosotherms (dashed) are in °C. At 500 mb, heights are solid where 591 denote 5910 m and temperatures (dashed) are in °C.

At 850 mb (Fig. 4), winds generally were light and variable over most of the southeastern United States. Wind plots (not shown) revealed convergence along the front over the Northern Plains, although there was little convergence along the Ohio Valley boundary. A moisture axis (dewpoints $\geq$ 15 °C) extended from North Dakota through the middle Mississippi River Valley.

RAOB-derived Lifted Indices (LI) at 1200 GMT are given in Fig. 5. Most of Kansas, Missouri, Arkansas, western Tennessee, and northern Mississipi were relatively unstable, with values less than 2. A smaller instability center was located over central Minnesota. On the other hand, the Great Lakes region was stable, with values greater than 10.

At 500 mb (Fig. 4) a strong developing trough stretched from southern Minnesota through central Missouri. Twelve hour height falls of 40 m could be found to its east. Strangely, however, the thermal analysis did not indicate a pronounced cold tongue behind or coincident with the height feature. Ridging extended ahead of the trough from Michigan to Tennessee, then west to a major center over Colorado. Using VAS profiles from the Smith (1983) algorithm, Fuelberg and Funk (1987) calculated large scale vertical motions for this case and found an area of upward motion to the east of the 500 mb trough.

Even higher, at 200 mb (not shown), a weak trough

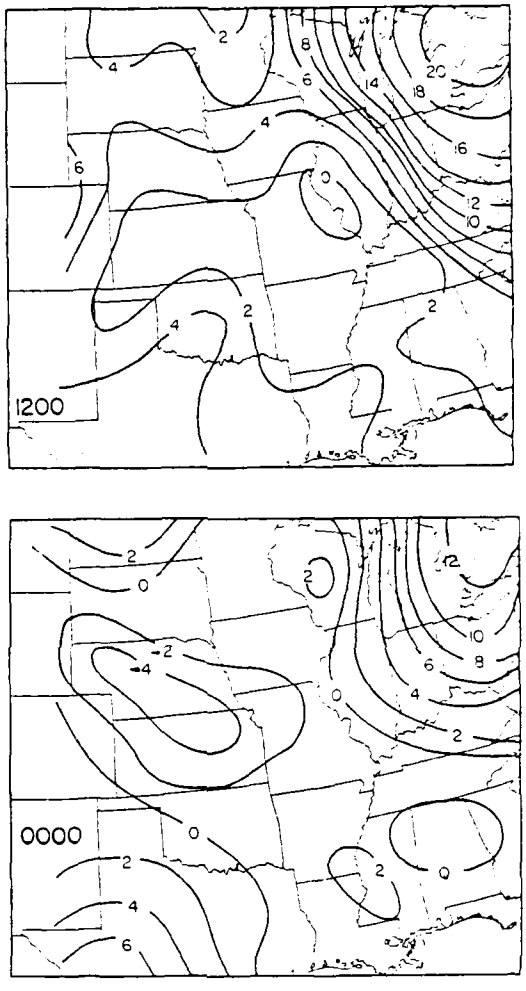


Fig. 5. Lifted Index at 1200 GMT 21 July and 0000 GMT 22 July 1982. Values were obtained from RAOBs.

stacked appropriately with its 500 mb counterpart; however, there was no well defined speed maximum nearby. With the exception of the weak short wave, flow generally was zonal over the entire region. Winds were stronger upwind of the trough, suggesting that further amplification was likely.

By mid-morning, i.e., 1600 GMT (Fig. 6), the cirrus debris over the Southeast had dissipated. Animated sequences of visible images revealed an apparent circulation over the Northern Plains which was moving southeastward into northeastern Iowa. Showers associated with the circulation drifted slowly to the east into Wisconsin. Elsewhere, showers and thunderstorms had developed over the northern half of Florida.

The 1800 GMT NMC surface chart (Fig. 7) showed a low pressure system over eastern Iowa, confirming the satellite-detected circulation center (Fig. 6). Attached to this surface low was a warm front over the Ohio River Valley which had earlier been classified as stationary. A surface streamline analysis (not shown) performed on the Florida State University Department of Meteorology's KLIMA (Kindly Local Interactive Meteorological Access) system revealed well defined convergence around the surface low. Similarly, KLIMA-derived analyses of surface moisture convergence indicated strong influx in the vicinity of the surface low and southeastward along the warm front.

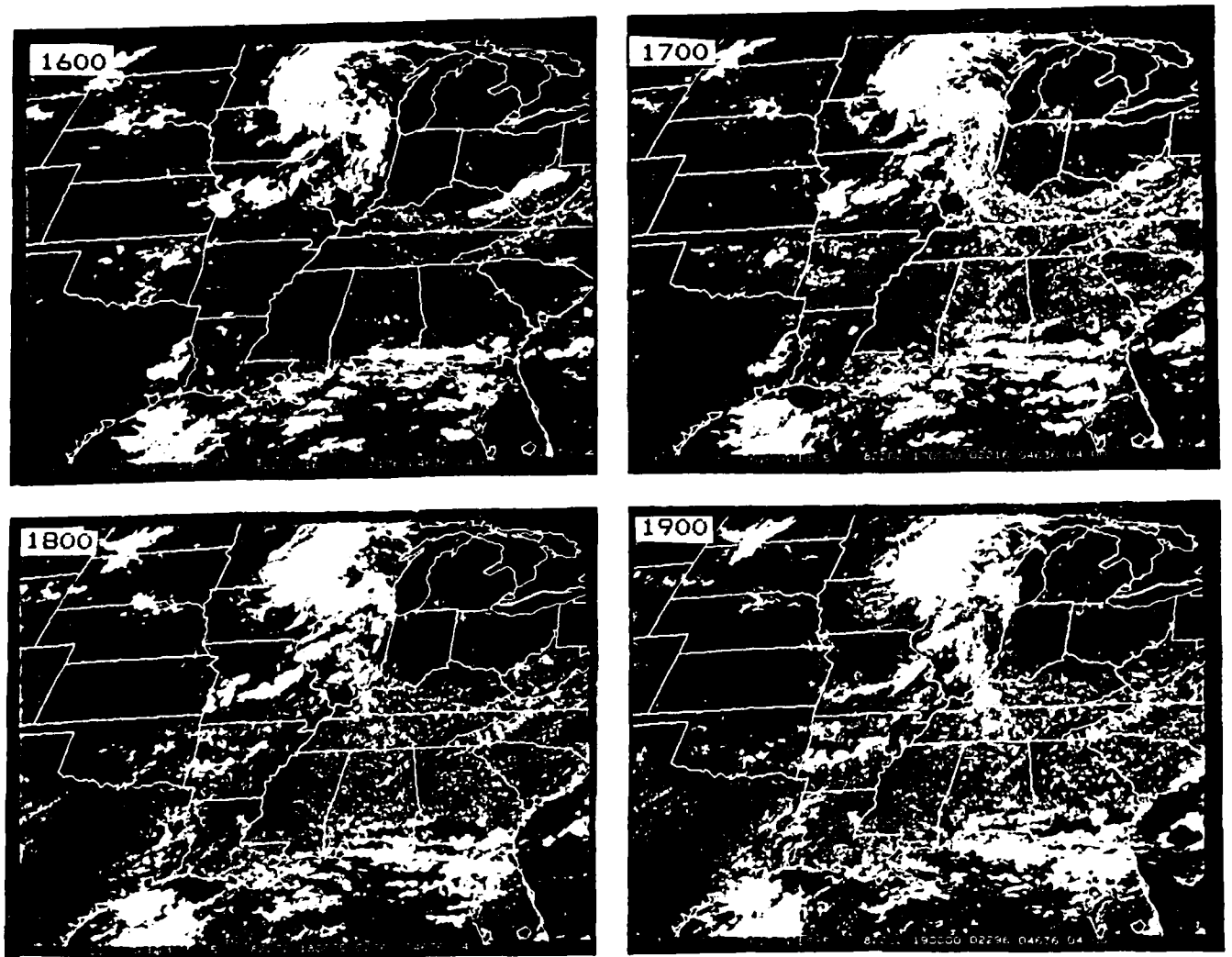


Fig. 6. Hourly visible satellite imagery between 1600 and 2300 GMT.

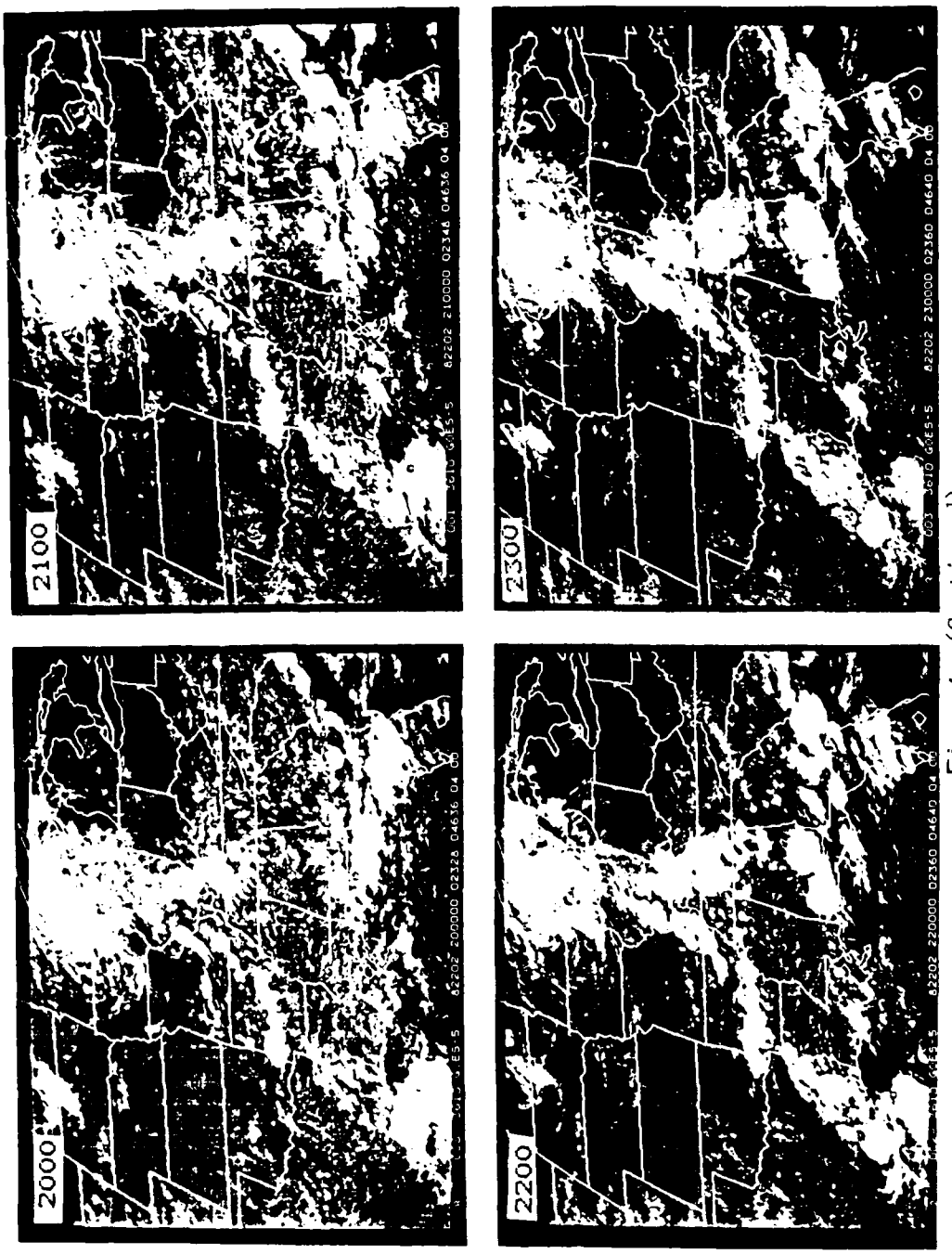


Fig. 6 (Continued)

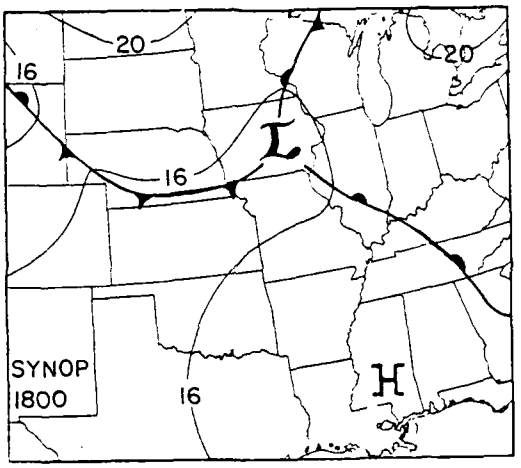


Fig. 7. Surface analysis at 1800 GMT 21 July.

During the afternoon hours, visible satellite imagery (Fig. 6) showed typical "popcorn" cumulus developing over most of the Southeast. Strong convection continued over northern Florida and southern Georgia, while clusters of new thunderstorms were developing over western Kentucky, central Arkansas, and southern Illinois by 1800 GMT. The latter two regions appeared to form along outflow boundaries from the nighttime thunderstorms in Missouri. A strong line of thunderstorms developed over southwestern Illinois (apparently along the warm front noted at 1800 GMT (Fig. 7)). The NSSFC issued a severe thunderstorm watch over most of Illinois for this developing line, and radar summaries (not shown) indicated tops exceeding 18 km during the late afternoon. Visible and infrared imagery suggested that the 500 mb trough had formed a cut-off low, with several small vorticity lobes rotating around it.

By 0000 GMT 22 July 1982, the NMC surface analysis (Fig. 8) indicated that the surface low had moved to northern Illinois. The cold front over the Plains had pushed southward to central Missouri, while a squall line was depicted over eastern Illinois. At 850 mb, the afternoon convection had distorted parts of the moisture field; however, the squall line continued to move with the moisture axis. Winds still were light and variable over most of the region, with only weak convergence noted along the Plains boundary.

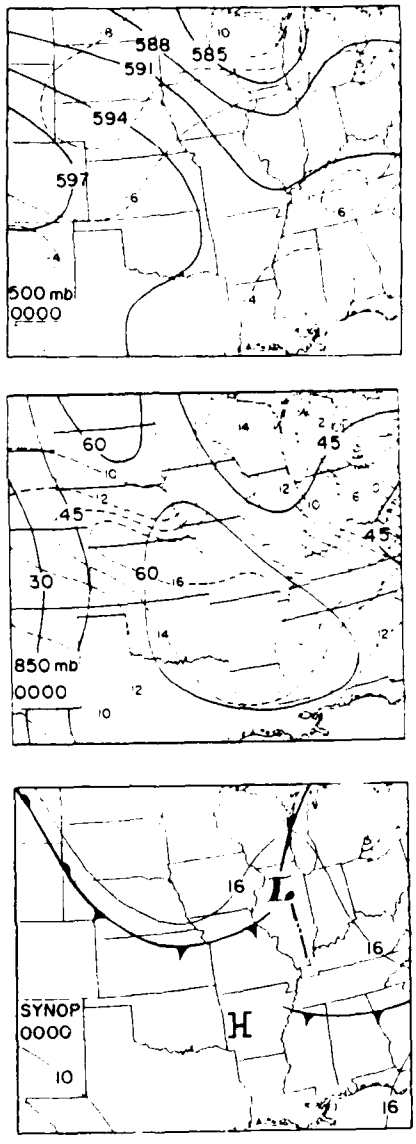


Fig. 8. As in Fig. 4, except at 0000 GMT 22 July.

The 0000 GMT LI analysis (Fig. 5) revealed that an area of instability had developed over central Nebraska and Kansas. Meanwhile, two other smaller instability centers were located over central Wisconsin and northern Alabama. The Great Lakes remained relatively stable, as values continued to exceed 10.

The 500 mb analysis (Fig. 8) indicated that the trough had indeed become cut-off, with the center just southwest of Green Bay, Wisconsin, and the trough trailing southward into central Illinois. The thermal field now was better defined, with a cold -10°C pocket located in the vicinity of the low. Conditions at 200 mb (not shown) were consistent with those at 500 mb and those seen 12 h earlier (Fig. 4).

In summary, 21 July was a "typical" summer day for severe weather, with reports of one tornado, two cases of large hail, and several instances of damaging wind reaching the NSSFC by late evening. Most of the severe activity was confined to the state of Illinois.

## 6. Data evaluations

One must understand the attributes and limitations of VAS soundings before using them to calculate derived atmospheric parameters. For example, do the data exhibit spatial and temporal continuity, i.e., is there good relative agreement between successive times and locations? Also, what are the magnitudes of bias errors, and how great is the "noise" (RMS errors)? Three approaches will be used to answer these questions. First, representative data plots will be examined, followed by point comparisons between VAS-derived and RAOB-derived soundings. Finally, using procedures similar to those of Fuelberg and Funk (1987), area averaged temporal characteristics will be presented.

For the purpose of retrieval assessment, temperature, dewpoint, and height data provided by the national RAOB network are assumed "perfect", i.e., they are considered to be the true atmospheric values at the time and location of the sensor. Of course, the radiosonde is <u>not</u> a "perfect" measuring device (Lenhard, 1970), and some of the VAS errors assumed from the calculations that follow actually will be attributable to this imperfect standard. Furthermore, as stated earlier, the sonde is a "point"

measuring device while the VAS instrument is a volume sensor.

Figs. 9 and 10 depict the evolution of VAS-derived 850 mb dewpoint and 500 mb temperature, respectively. The author performed the subjective analyses using standard meteorological techniques learned as a severe weather forecaster at the Air Force Global Weather Central (AFGWC). Where possible, ridges, troughs, moisture axes, etc., were enhanced without conflicting with the data, i.e., all data were retained in the analysis. As can be seen, both isotherms and isodrosotherms are relatively smooth with no discontinuities.

The VAS humidity patterns at 850 mb (Fig. 9) contain several interesting features. The moisture axis initially stretching from southern Minnesota to the central Gulf Coast has reasonable continuity. Specifically, there is a slight eastward progression throughout the afternoon hours, and its relative strength remains fairly constant at 16-18°C. Much drier conditions are found over the northeast corner, i.e., on the cold side of the frontal system located over the Ohio River Valley (Figs. 4, 7, 8). Especially interesting is the development of a relatively small scale "dry" pocket in the Missouri-Illinois area between 1600-1700 GMT. This feature will be examined in greater detail in a later chapter.

In general, the broad scale aspects of VAS-derived

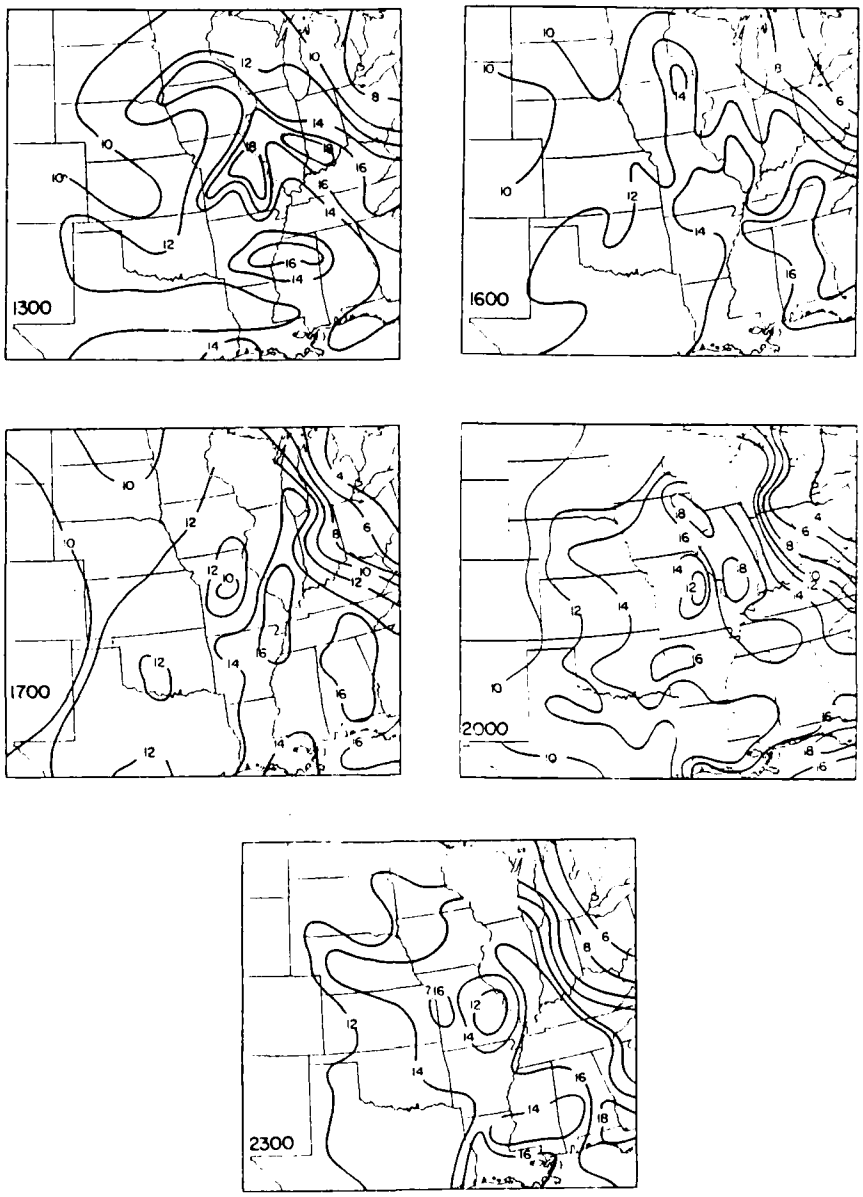


Fig. 9. VAS-derived dewpoint analyses at 850 mb (°C). Times are GMT on 21 July.

dewpoint patterns at 1300 and 2300 GMT (Fig. 9) are closely related to sonde-derived versions at 1200 and 0000 GMT (Figs. 4 and 8, respectively). Agreement between the moisture axis over the Mississippi River Valley is the prime example. It is clear that the closer spacing of the VAS retrievals has provided considerably smaller scale resolution of features than is possible from the radiosonde network. On the other hand, values at individual RAOB sites sometimes differ between the two data types. This aspect is explored in later paragraphs.

Although the satellite's 500 mb temperature fields (Fig. 10) are not as well defined as the just described 850 mb dewpoints, several features do exhibit good continuity. For example, a cold trough initially over Iowa moves eastward and out of the data domain during the afternoon. Unfortunately, since it is located near a cloud induced data gap (Fig. 3), one cannot have great confidence in its exact location or minimum temperature. A second cold axis consistently located over Nebraska is more pronounced by the ending time. Finally, a cold pocket over southern Georgia is quasi-stationary. Once again, broad scale features of the VAS analyses have similarities to those from the standard source (Figs. 4, 8). Also, VAS temperatures vary several degrees from one time to another.

In order to estimate the accuracy of VAS measurements,

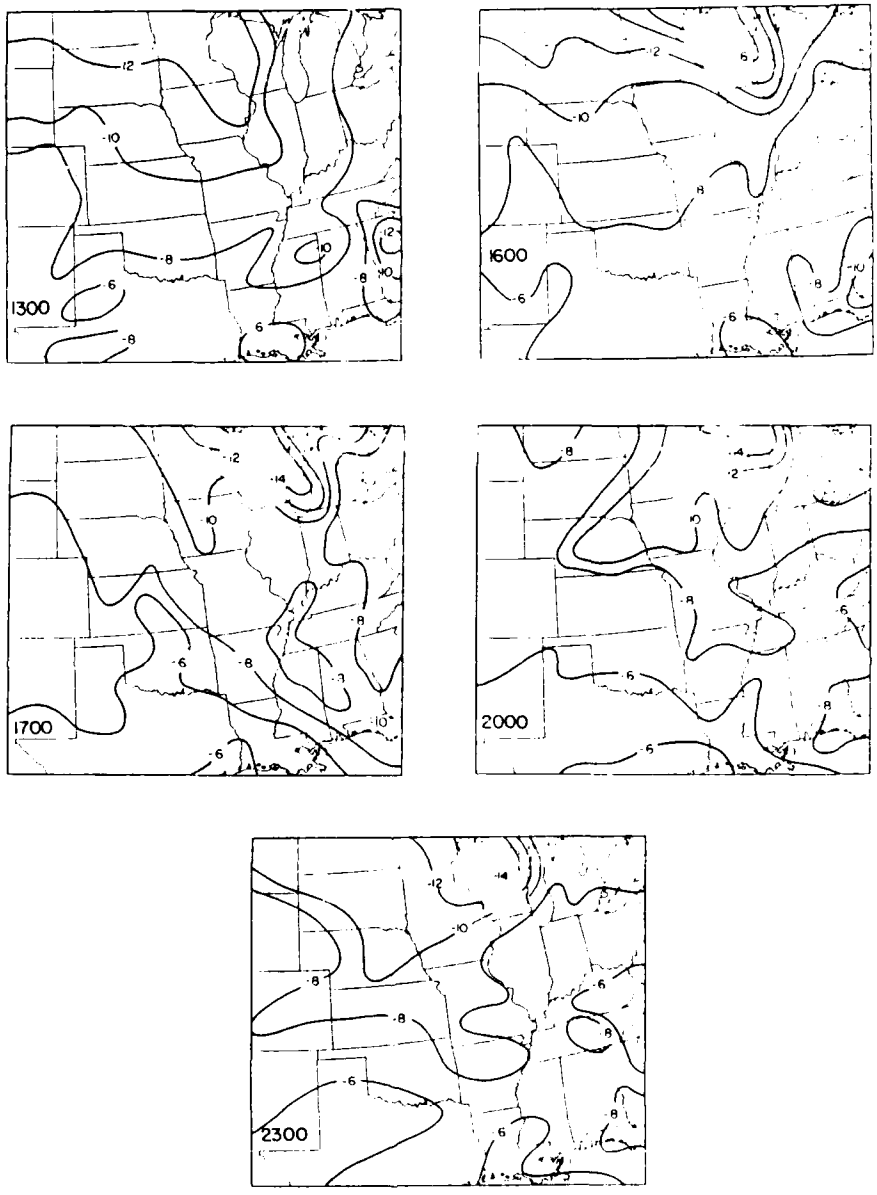


Fig. 10. VAS-derived temperature analyses at 500 mb (°C). Times are GMT on 21 July.

retrievals were paired with nearby radiosonde-derived "ground truth" data. Then, the VAS-derived values were subtracted from the sonde-derived measurements. This procedure is similar to that employed by previous authors, e.g., Phillips *et al.* (1979), Gruber *et al.* (1982). Three criteria had to be met for each comparison. First, the VAS profile being paired had to be within a 100 km radius of the RAOB location. Second, the 100 km criterion had to be met at both the 1200 and 0000 GMT RAOB sounding times. Third, the same RAOB sites had to be available in evaluating both the simultaneous and the physical retrievals, i.e., the same numbers and locations of RAOBs. There are at least two unavoidable limitations to the pairing procedure. First, although the 100 km value was required to obtain a sufficient number of pairings, structure function analyses of radiosonde and VAS data have showed that appreciable horizontal gradients still exist at scales smaller than 100 km, especially for water vapor (Fuelberg and Meyer, 1985). Second, there was a 0-2 h difference between the two data sources, i.e., 1200 GMT RAOBs (released near 1100 GMT) were compared to 1300 GMT VAS profiles, and 0000 GMT RAOBs (released near 2300 GMT) were compared to 2300 GMT VAS locations. Thus, this lack of complete spatial and temporal agreement will be a source for some of the calculated discrepancies that are described next.

Table 3 gives results for both the simultaneous and older physical retrievals (used originally by Fuelberg and Funk, 1987). Seven RAOB-VAS data pairs met the three criteria. These relatively small sample sizes are a limitation to the evaluation. It was possible to obtain 16 RAOB-VAS pairings for the simultaneous retrievals by dropping the third criterion; however, those results (not shown) are similar to those of the smaller sample size (Table 3). For comparison purposes, previously published results for the older algorithm (Jedlovec, 1985) and the new algorithm (Wade *et al.*, 1985) also are included in the Table.

The simultaneous (new) algorithm appears to provide better estimates of water vapor profiles (Table 3); however, the temperature soundings are inferior to those of the older approach. Specifically, mean dewpoint bias errors for the simultaneous retrievals are considerably smaller than those from the physical algorithm. Both procedures yield dewpoints that are warmer (positive bias) than RAOBs in the lower troposphere, but colder aloft. RMS errors for the simultaneous retrievals are comparable to those of the older approach at 850 and 700 mb, but the newer results clearly are superior at the higher levels. Current simultaneous mean bias errors are smaller than those of Jedlovec (1985), but there is no consistent relation with his RMS errors. In addition, simultaneous

Table 3. A comparison of VAS retrievals paired with nearby RAOBs. The leftmost value of each entry is the mean error while the rightmost value is RMS error. Units are °C for dewpoint and temperature and m for height.

| | Simultaneous | | Physical | |
|---|---|---|---|---|
| Pressure level (mb) | This study | Wade et al. (1985) | This study | Jedlovec (1985) |
| | | **Dewpoint** | | |
| 300 | -3.6/4.4 | | -6.5/8.3 | |
| 400 | -2.2/4.4 | | -7.6/6.3 | 4.0/3.6 |
| 500 | 0.8/4.4 | | -9.2/5.4 | -2.4/4.6 |
| 700 | 2.0/4.7 | | 4.9/4.3 | -5.9/5.5 |
| 850 | 0.3/3.3 | 0.4/7.8 | 4.3/3.1 | -1.8/2.3 |
| | | **Temperature** | | |
| 200 | -4.0/1.5 | | -1.9/1.7 | -0.1/1.3 |
| 300 | -3.3/1.7 | | -1.5/2.0 | -1.7/1.6 |
| 400 | -2.9/1.5 | | -2.0/2.3 | -1.7/1.4 |
| 500 | -1.5/1.7 | 0.3/1.8 | -1.5/1.3 | -1.7/1.6 |
| 700 | 1.9/2.2 | | 0.2/2.2 | 0.4/1.1 |
| 850 | 2.2/2.0 | 0.9/2.3 | 0.5/2.0 | -2.5/1.5 |
| | | **Height** | | |
| 200 | -42.8/37.5 | | -17.1/37.3 | -42.0/21.0 |
| 300 | -9.4/36.3 | | 1.6/23.4 | -31.0/21.0 |
| 400 | 9.3/36.7 | | 3.1/16.9 | -13.0/18.0 |
| 500 | 19.2/34.8 | | 10.1/16.2 | -4.8/12.0 |
| 700 | 9.4/18.9 | | 8.9/ 9.7 | 4.2/ 7.9 |
| 850 | -3.0/10.3 | | 3.4/ 5.5 | 4.3/ 6.8 |

errors at 850 mb are smaller than those of Wade *et al.* (1985).

The greatest dewpoint difference (simultaneous retrievals) at a single level occurred over Denver at 300 mb (-20.6°C). Fig. 11 (12) displays the "best" ("worst") dewpoint profile, i.e., considering the entire sounding. Errors averaged 2.0 °C at each level for the "best" sounding, but exceeded 10°C between the surface and 400 mb for the "worst" case. The reduced vertical resolution of the VAS retrievals is clearly evident. Furthermore, it is interesting that VAS-derived dewpoint retrievals having good agreements with the RAOB versions often correspond to temperature profiles differing greatly from those of the sondes, and vice versa. As an extreme example, the pairing which exhibits the best overall dewpoint agreement (Fig. 11) also has the worst temperature comparison.

When temperatures from the two algorithms are compared with RAOBs (Table 3), the simultaneous version exhibits increased magnitudes of mean error. The new soundings tend to be slightly warmer than RAOBs in the lower troposphere; however, the bias becomes negative (cooler) by the 500 mb level, increasing to -4.0°C at 200 mb. This tendency is consistent with that of the older physical retrievals. RMS errors vary little with altitude and are approximately 1.7 °C for both sets of soundings. The greatest temperature error at a single level also occured in the Denver profile

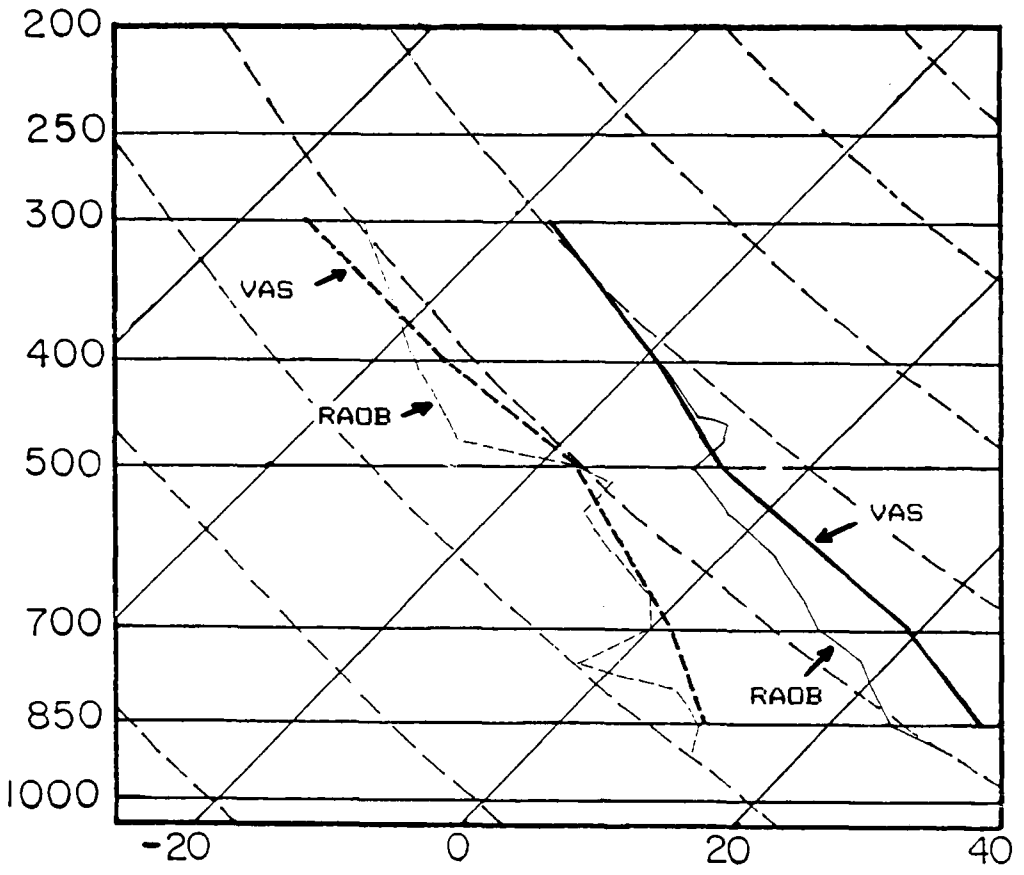


Fig. 11. Skew T-log P diagram of the VAS [illegible] having the worst temperature [illegible] agreement with its nearby radiosonde [illegible] also had the best agreement [illegible] point temperatures. The location [illegible] Rapid City at 2300 GMT. Solid [illegible] represent VAS, RAOB [illegible].

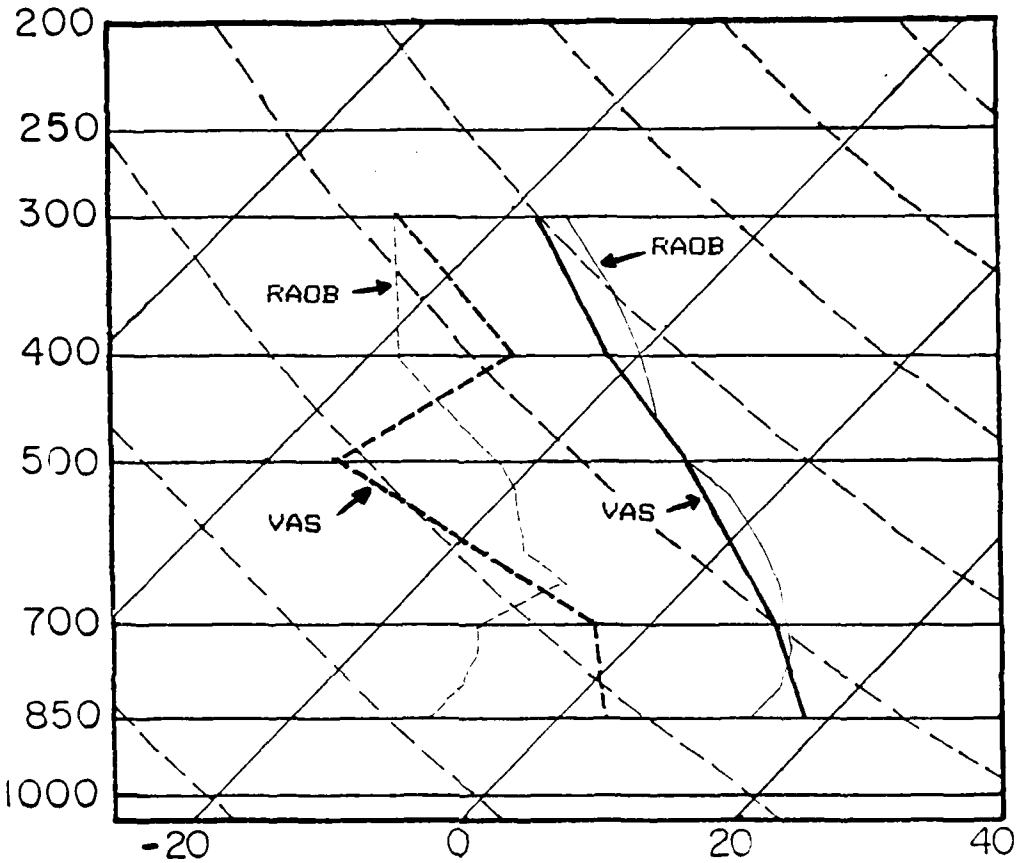


Fig. 12. As in Fig. 11, except for the ... dent between dewpoints. ... near Buffalo at 2300 ... lines represent VAS ...

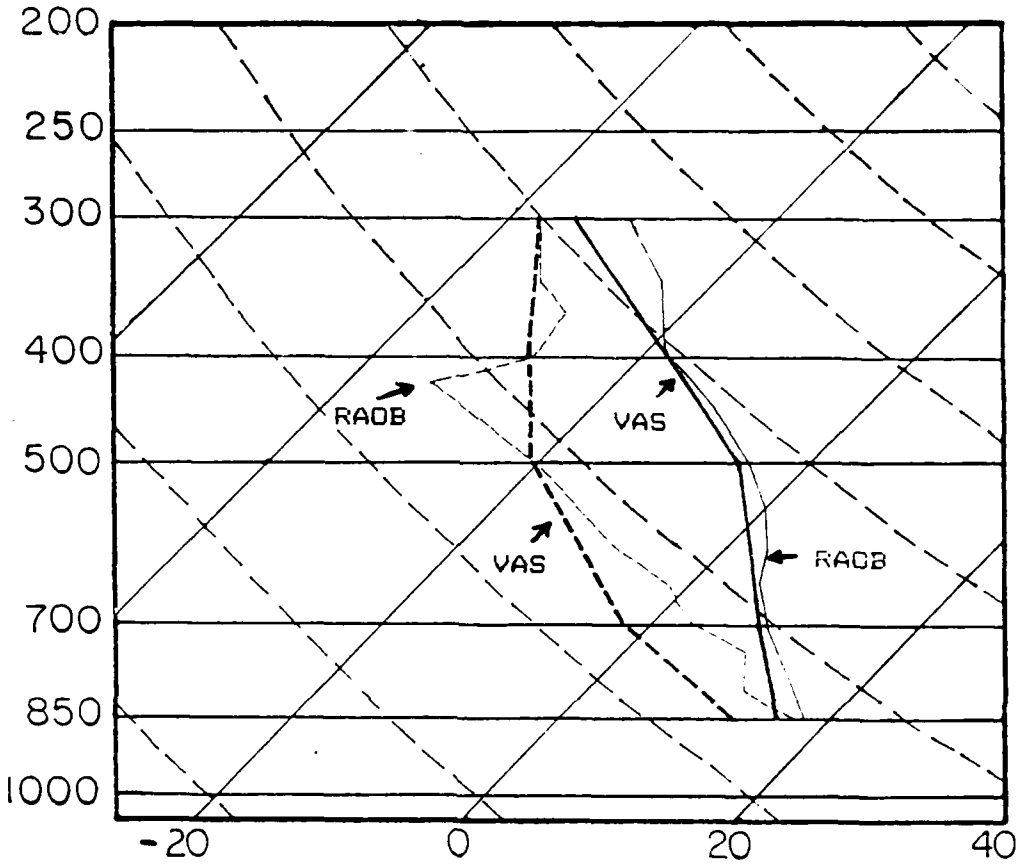


Fig 13. As in Fig. 11, except for [illegible] ment between temperature [illegible] near Charleston at [illegible] lines represent VAS [illegible]

at 300 mb (+8.4 °C). Fig. 13 (11) shows the "best" ("worst") VAS/RAOB temperature comparisons. Errors at each level are 1.0°C ( 4.0°C) from 400 mb to the surface for the "best" ("worst") sounding.

Since heights are obtained by integrating temperature and dewpoint through the hypsometric equation, biases for height correspond to those of the temperatures (Table 3). Greatest positive bias occurs at 500 mb in both cases, but values rapidly become negative at higher levels. Greatest negative biases occur at 200 mb. The increasingly large negative values in the upper troposphere result from the cold bias. RMS errors for the simultaneous retrievals often are twice those from the physical version.

Although the newer algorithm produces smaller mean and RMS dewpoint errors, it is disconcerting that the mean temperature errors are greater. Dr. C. M. Hayden of NESDIS has kindly provided an explanation for this phenomenon (personal communication, 1987). Specifically, the VAS radiometer now is known to produce biased radiances, possibly due to temperature variations on its filter wheel. To control the mean retrieval errors that result from this input, NESDIS alters the radiances. These radiance corrections had been updated weekly, but future plans call for daily updates. Based on the increased mean temperature bias (Table 3), it is assumed that radiance

corrections applied when the simultaneous retrievals were prepared in 1985 are not the same as those used in creating the older physical version in 1982. This aspect of the retrieval process underscores the importance of emphasizing VAS-derived patterns at single times and pattern evolutions over short periods. Conversely, one should not stress magnitudes of VAS products at individual locations or their comparison with RAOBs. This aspect has been noted operationally by personnel at NSSFC (Anthony and Wade, 1983).

Fuelberg and Funk (1987) calculated mean soundings within several geographic "boxes" over the midwestern United States in order to describe temporal variations in the physical retrievals. To compare performance changes between the two algorithms, similar boxes were chosen (Fig. 14) for this study. Box "A" enclosed a large area which was relatively cloud-free during the entire day, while Box "B" was centered over an area which experienced strong afternoon convection. Using simple averaging, a mean profile was created for each box at each time. For Box A, approximately 30 soundings from the new algorithm were averaged at each time, whereas there were 40 from the older algorithm. The averages for Box B consisted of approximately 15 (20) soundings for each time from the new (old) data. To clearly reveal the temporal tendencies, area-averaged profiles at consecutive times were

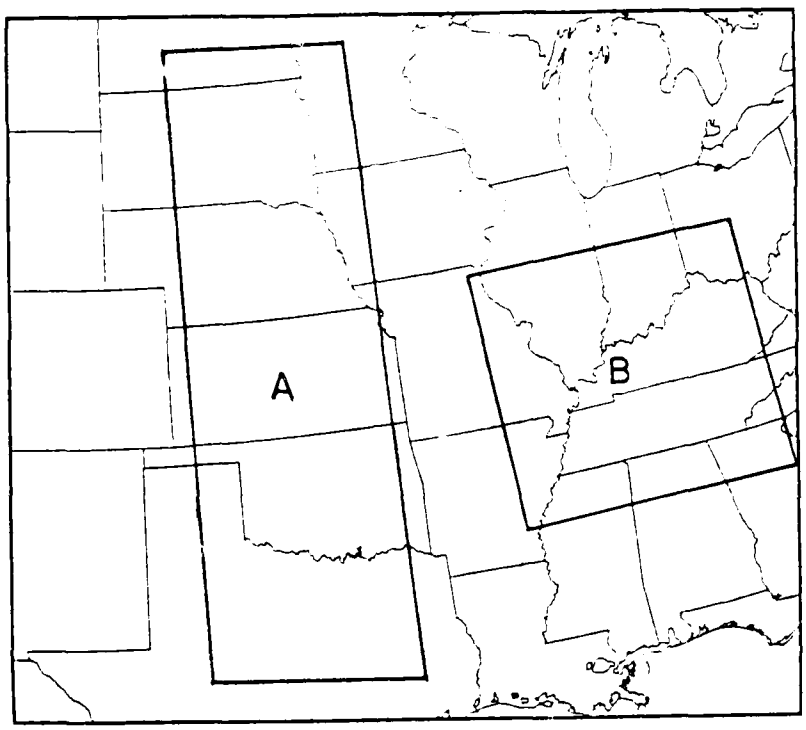


Fig. 14. Regions over which area-averaged retrievals were calculated.

subtracted from each other. For the sake of brevity, only results from the 1300-1600 GMT (Fig. 15) and 2000-2300 GMT (Fig. 16) calculations are presented here. For comparison purposes, results from Fuelberg and Funk (1987) also are plotted.

Fuelberg and Funk (1987) noted that physically-derived temperatures from near the surface to approximately 400 mb exhibited strong warming during the morning (Fig. 15), but there was compensating cooling at higher levels. These trends reversed during the afternoon (Fig. 16). The variations could not be explained from temperature advection, and one would not suspect daily surface heating to affect levels much above the boundary layer. Therefore, they mostly attributed the unrealistic trends to deficiencies in the retrieval algorithm. With the newer soundings, the simultaneous algorithm performs considerable better during the afternoon (Fig. 16); however, there still are major variations during the morning (Fig. 15) that appear to be algorithm related.

The area averaged dewpoint profiles of Fuelberg and Funk (1987) exhibited tendencies similar to those of temperature (Figs. 15, 16). That is, morning values increased (decreased) in the lower (upper) troposphere, and there was a reversal between morning and afternoon. Since there was no meteorological explanation for the variations, it appeared that humidity calculations were

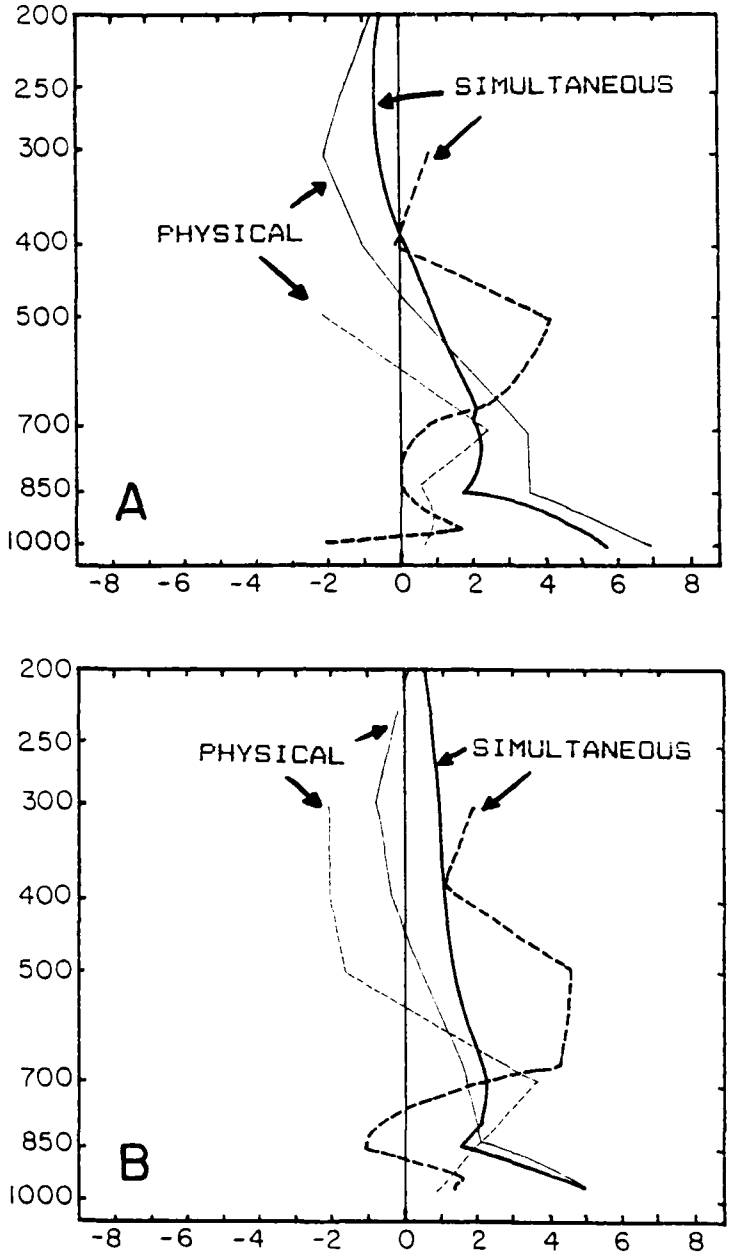


Fig. 15 Change in area-averaged temperature and dewpoint (°C) between 1300 and [illegible] GMT. Solid and thin dashed lines represent simultaneous observed [illegible]

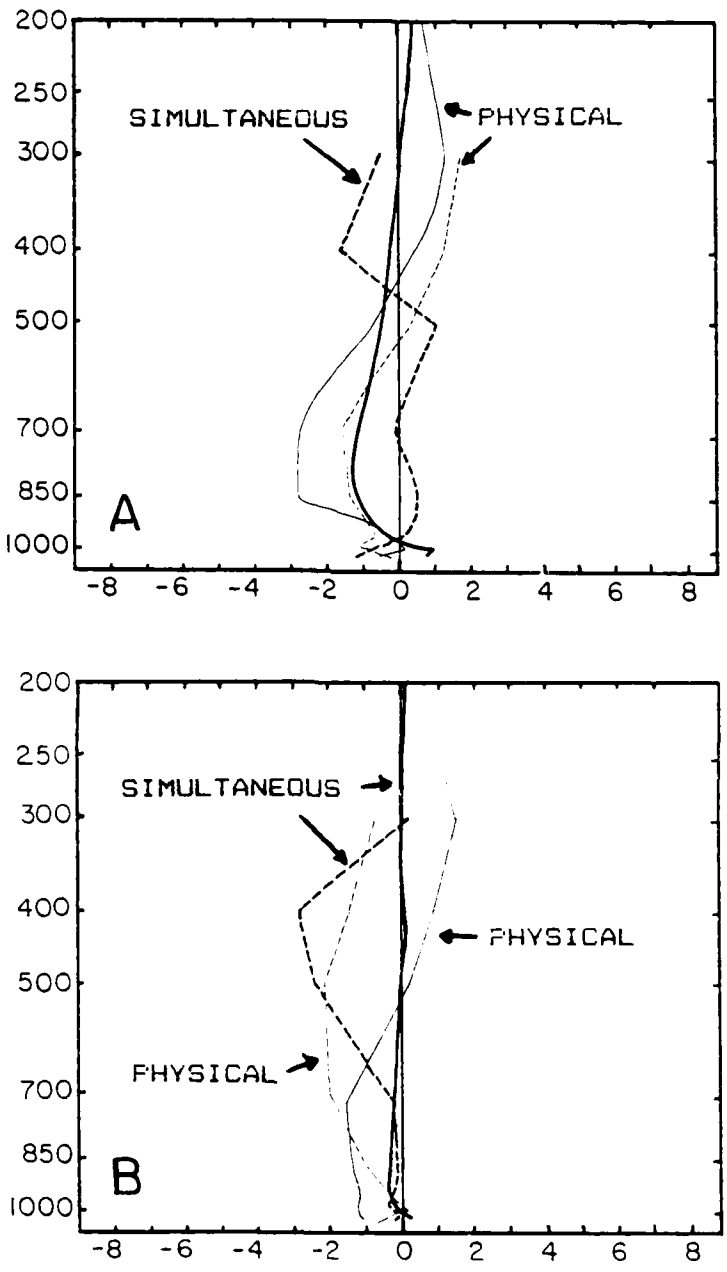


Fig. 16. As in Fig. 13. Initial [illegible] 2300 GMT. [illegible] physical [illegible] profiles.

closely related to the questionable temperatures. With the newer simultaneous retrievals (Figs. 15, 16), unrealistic trends remain. Specifically, there is a large increase (3 - 4 °C) in mid-level moisture during the morning hours followed by drying in the afternoon, but again this cannot be substantiated by satellite imagery or conventional data.

In summary, from the standpoint of accuracy, the new simultaneous algorithm should be rated better than the Smith (1983) scheme. Moisture values are closer to the "truth", although temperature accuracy is slightly worse. Diurnal variations have been reduced, but not eliminated, and some of the compensating effects have been removed. Armed with this information about the basic data, several different thermodynamic parameters related to severe storm forecasting will be presented in the following chapters.

## 7. Non-integrated stability parameters

Summer is the most difficult season for forecasting the location and intensity of convection because the atmosphere generally is sufficiently unstable for even minor ascent ("trigger" mechanisms) to initiate possible severe storm activity. A meteorologist needs to know the patterns of atmospheric stability together with a knowledge of the vertical motion. Synoptic scale and mesoscale "triggers" on 21 July were described in Chapter 5; this chapter considers stability.

Several thermodynamic indexes are used by operational meteorologists to evaluate stability. They usually are derived from input at various atmospheric levels and can be placed into two distinct groups, integrated and non-integrated. The integrated variety is based on numerous data over a thick layer, rather than measurements at a few discrete levels (the non-integrated type). Examples of integrated parameters include precipitable water and buoyant energy. This chapter will deal with the non-integrated parameters, specifically, the Lifted Index (LI), K Index (KI), and Total Totals (TT) Index.

### a. Lifted index

The LI is the most widely used stability index of the National Weather Service and is calculated every 12 h from all RAOBs in the United States. The LI is based on a temperature comparison between a saturated parcel which has been lifted adiabatically to 500 mb and the actual 500 mb sounding temperature. The parcel temperature is subtracted from the sounding temperature to produce the index value. When the parcel is warmer than the environment (negative index), the atmosphere is considered unstable. An atmosphere with an LI of -4 or less is classified as having severe storm potential. Temporal variations in LI also provide useful information. Thus, the NSSFC calculates hourly changes in LI by blending surface data with the 12 h RAOBs (Hales and Doswell, 1982), thereby helping forecasters pinpoint areas of severe weather potential.

There are a variety of schemes for calculating LIs, with differences mainly due to the method of initially specifying the parcel. The LI values presented in this paper were based on the following algorithm: First, the mean temperature and dewpoint were calculated for the lowest kilometer by using simple averaging of all retrieved values in that layer. One may argue that this negates inclusion into the non-integration category; however, the layer is much more shallow than employed in the integrated variety described later. After mean values

were determined, the Lifting Condensation Level (LCL) was computed by raising the parcel dry adiabatically until saturation. Then, the parcel was cooled moist adiabatically to 500 mb where the temperature comparison was made.

Fig. 17 displays fields of VAS-derived LI for the five observation times. As with the dewpoint analyses described earlier (Fig. 9), the LIs have good spatial and temporal continuity. Several features in the 1300 GMT field undergo interesting evolutions that should be discussed in detail. First, the relative minimum (unstable) in eastern Missouri (-6) slightly loses intensity during the day, becoming as stable as -3. The area becomes a well defined relative maximum (more stable) by 2000 GMT and continuing to 2300 GMT mostly because the surrounding areas become much less stable. The comparitive afternoon stability over eastern Missouri appears due to early morning convection in the area. Specifically, a strong outflow boundary was evident in satellite imagery (Fig. 6), suggesting drier, downdraft air from the early morning storms. This is reflected in the 850 mb dewpoint fields at 1700 GMT (Fig. 9) by a relative minimum (-10°C) over eastern Missouri. This drier region at 850 mb is consistent with that from routine surface data (not shown). Thus, VAS suggests that the apparent downdraft air is not confined merely to the boundary layer.

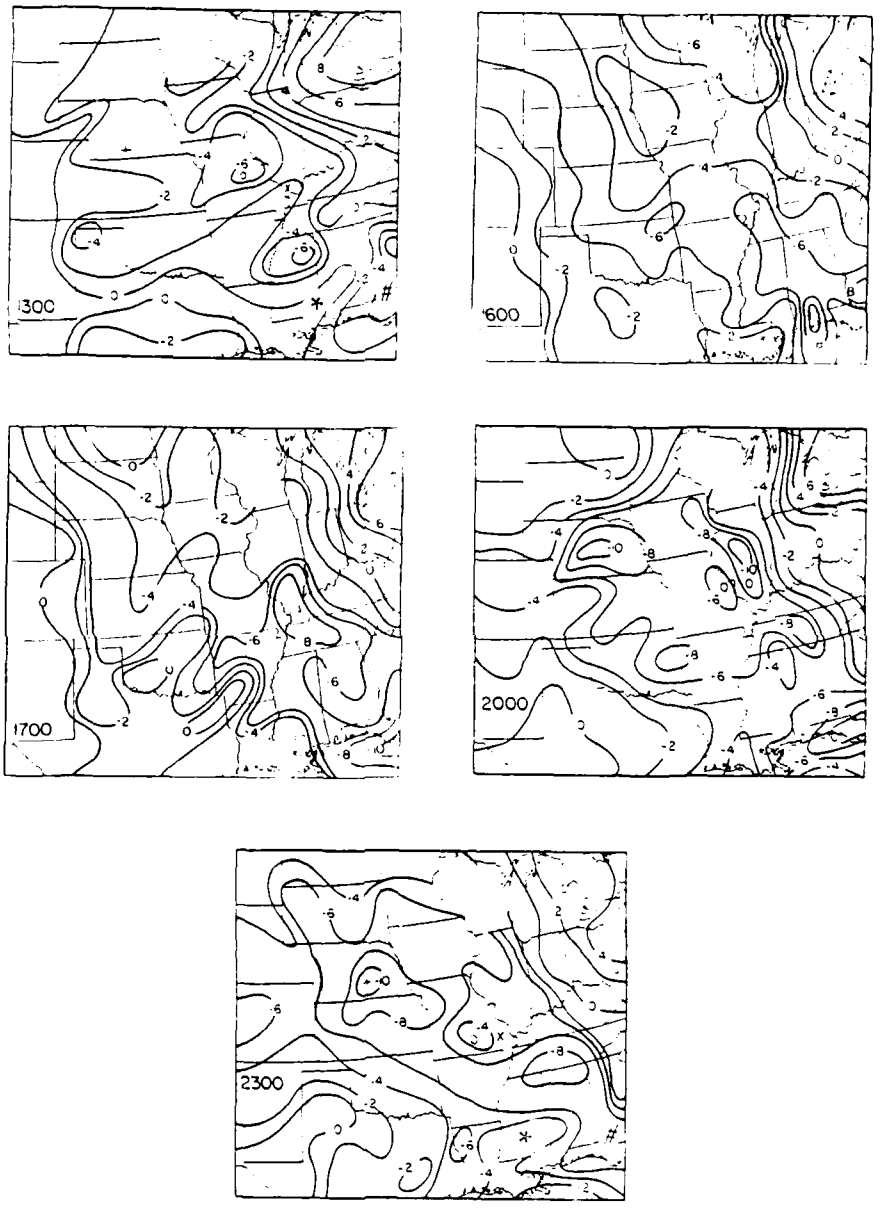


Fig. 17. VAS-derived Lifted Indexes at the five observation times.

To further explore the apparent outflow, VAS retrievals for the area are given in Fig. 18; actual sounding locations are noted in Fig. 17 by the symbol O. Profiles east and west of the boundary at 2000 GMT (Fig. 18a) reveal marked drying from the ground to the middle troposphere west of the boundary. Examination of profiles at 1300 and 2300 GMT (Fig. 18b) reveals a large daytime decrease in dewpoint from the surface to near 600 mb. The slight increase in moisture in the middle troposphere might be a result of the convection, i.e., debris. The dry low level air would limit further storm development over the area, and this is confirmed by satellite imagery indicating no convection over Missouri after 1700 GMT. Strong diurnal warming is noted near the surface, however the 2-3°C increases above 850 mb are suspect.

Another evolving feature at 1300 GMT (Fig. 17) is the relative minimum (-6) in northern Mississippi which seems to migrate northward throughout the day. Values reach -8 at 1700 GMT, and -10 by 2000 GMT, before diminishing at 2300 GMT due to the storms over Illinois. As noted earlier (Chapter 5) this was the area of the most intense afternoon convection (Fig. 6). To explore the rapidly changing stability, VAS-derived soundings for 1300 and 2000 GMT over southern Illinois (Fig. 19) are examined. Once again, their locations are given in Fig. 17, this time by Xs. The LIs for these soundings change from -1 at

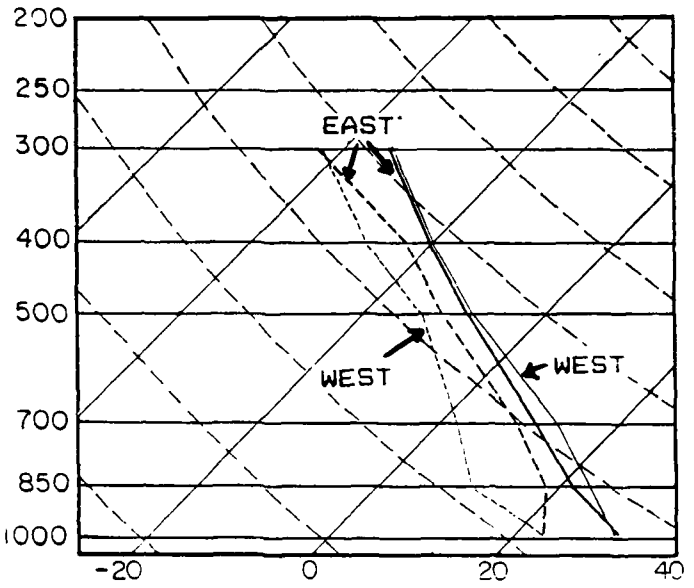


Fig. 18 .. AS retrievals east (bold) and ... of the outflow ... Missouri at 2000 GMT. Sounding ... are given by the symbol O in Fig. ...

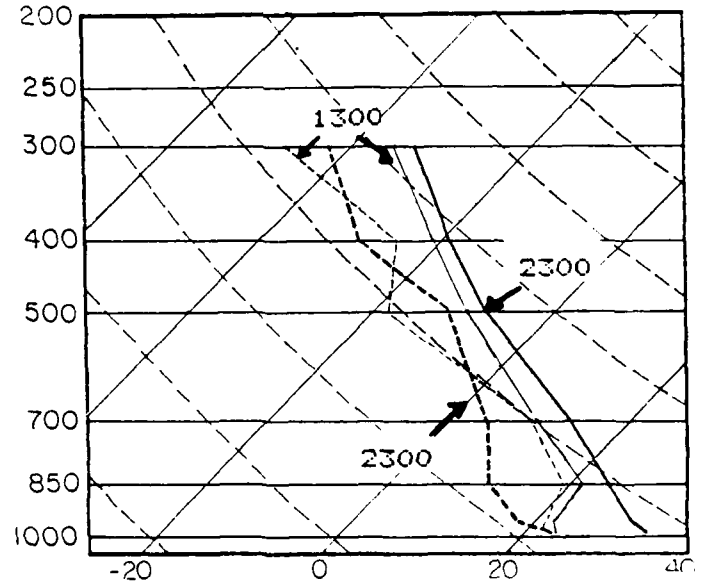


Fig. 19 .. ... retrievals over Missouri ... and ... of ... ... given by the symbol ...

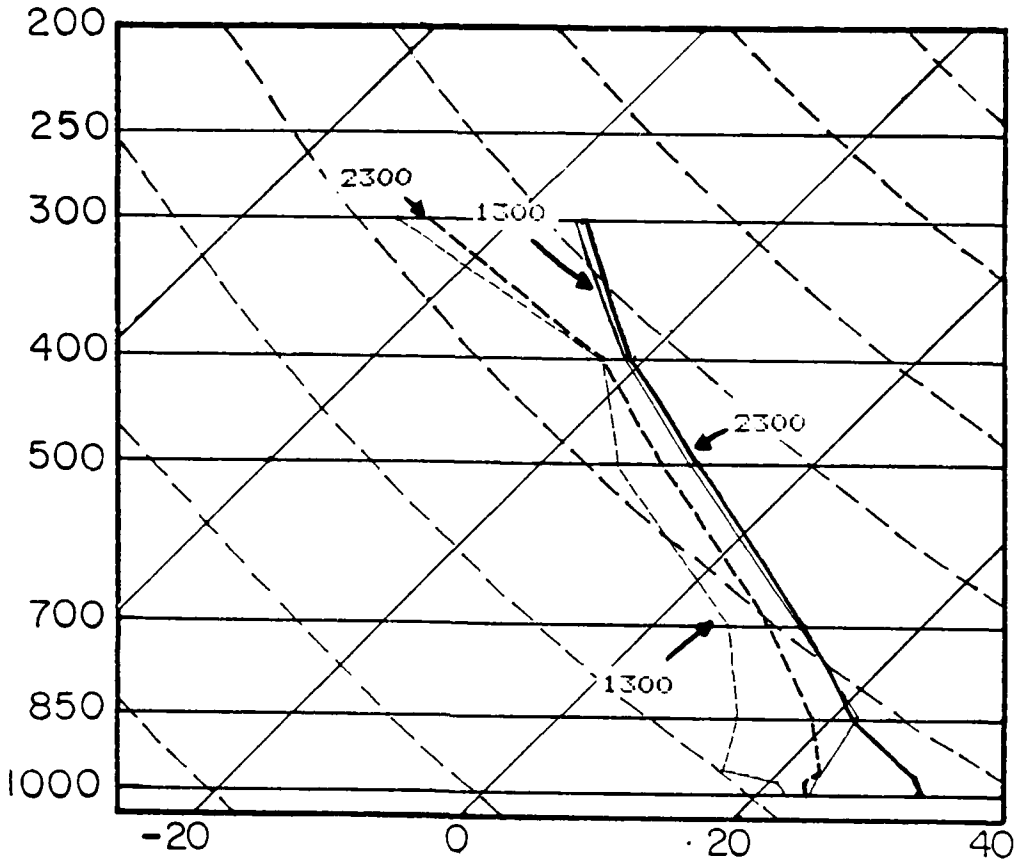


Fig. 19. VAS retrievals over southern Illinois at 1300 (thin) and 2300 GMT (bold). Sounding locations are given by the symbol X in Fig. 17.

@A186158 U FIELD/GROUP @@@@@@

UNCLASSIFIED TITLE
ASSESSMENT OF VAS-DERIVED PRODUCTS CREATED BY A SIMULTANEOUS ALGORITHM ON A CONVECTIVELY ACTIVE DAY.

ABSTRACT
(U) GOES-VAS SATELLITE RETRIEVALS CREATED BY A NEW SIMULTANEOUS ALGORITHM ARE EXAMINED. THE GOALS ARE TO DETERMINE THE SPATIAL AND TEMPORAL CHARACTERISTICS OF THE DATA, AS WELL AS THE MAGNITUDES OF MEAN AND RMS ERRORS. SEVERAL INTEGRATED AND NON-INTEGRATED STABILITY PARAMETERS ARE EXAMINED TO ASSESS VAS'S CAPABILITY FOR PROVIDING USEFUL INFORMATION IN CONVECTIVE STORMS FORECASTING. THE IMPROVED MOISTURE INFORMATION HAS A POSITIVE IMPACT ON VARIOUS STABILITY INDICES. A VAS-DERIVED LIFTED INDEX APPEARS TO BE A PROMISING CONVECTION FORECAST TOOL. MANY SMALL SCALE FEATURES IN SATELLITE IMAGERY WERE RELATED TO THE LIFTED INDEX ANALYSES. ALSO, THE VAS-DERIVED VALUES PROVIDED INFORMATION THAT COULD NOT BE OBTAINED FROM CONVENTIONAL SURFACE DATA. THE K INDEX AND TOTALS INDEX ALSO PROVIDED FORECAST DATA; HOWEVER, THEIR RESOLUTION DID NOT APPEAR AS GOOD AS THOSE OF THE LIFTED INDEX. INTEGRATED VALUES OF POSITIVE AND NEGATIVE ENERGIES WERE CALCULATED, AS WEELL AS THE HEATING ENERGY REQUIRED TO RAISE THE SURFACE TEMPERATURE TO ITS CONVECTIVE VALUE. THE POSITIVE BUOYANT ENERGY ANALYSES WERE SIMILIAR TO THE LIFTED INDEX FIELDS, WHILE THE NEGATIVE ENERGY PATTERNS APPEARED TO LOCATE THE LID TO CONVECTIVE ACTIVITY, THEREBY PROVIDING A FORECASTER WITH AN ADDITIONAL PREDICTION TOOL.

POSTING TERMS ASSIGNED

CONVECTION FORECAST TOOL
USE CONVECTION FORECASTING

CONVECTIVE ACTIVITY
USE CONVECTION

CONVECTIVE STORMS FORECASTING
USE CONVECTION(ATMOSPHERIC) FORECASTING/STORMS

CONVECTIVE VALUE
USE CONVECTION

CONVENTIONAL SURFACE DATA
USE SURFACES

FORECAST DATA
USE FORECASTING

HEATING ENERGY
USE ENERGY HEATING

INDEX ANALYSES
USE INDEXES

INDEX FIELDS
USE INDEXES

INTEGRATED STABILITY PARAMETERS
USE INTEGRATED SYSTEMS STABILITY

INTEGRATED VALUES
USE INTEGRATED SYSTEMS

MOISTURE INFORMATION
USE MOISTURE

NEGATIVE ENERGIES

NEGATIVE ENERGY PATTERNS

USE ENERGY

NEW SIMULTANEOUS ALGORITHM
USE ALGORITHMS
SYNCHRONISM

POSITIVE BUOYANT ENERGY ANALYSES
USE BUOYANCY
ENERGY

PREDICTION TOOL
USE PREDICTIONS

SIMULTANEOUS ALGORITHM
USE ALGORITHMS
SYNCHRONISM

SURFACE TEMPERATURE
USE SURFACE TEMPERATURE

USE ENERGY
PATTERNS

NON-INTEGRATED STABILITY PARAMETERS
USE STABILITY

POSITIVE IMPACT
USE IMPACT

SATELLITE IMAGERY
USE IMAGES
SATELLITE PHOTOGRAPHY

STABILITY INDICES
USE INDEXES
STABILITY

PHRASES NOT FOUND DURING LEXICAL DICTIONARY MATCH PROCESS

1300 GMT to -9 at 2000 GMT. The morning profile exhibits the classic severe weather pattern, i.e., a shallow moist layer near the surface capped by an inversion and drier air aloft. In the afternoon sounding, VAS indicates that surface diabatic heating has destroyed the morning inversion, while moisture has increased from the surface to near 400 mb. With the exception of the boundary layer, temperatures are relatively static during the 7 h time period; however, slight cooling is suggested above 500 mb, thereby agreeing with the RAOB analyses (Figs. 4, 8). The 1700 and 2000 GMT LI fields (Fig. 17) clearly provide the forecaster with excellent guidance since the strong (severe) convection forms in the minimum areas (-8) defined by VAS from southern Illinois to western Tennessee.

The morning and afternoon convection over southern Georgia and northern Florida (Fig. 6) occurs near another LI minimum, -6 at 1300 GMT (Fig. 17). This region shifts slowly toward the southwest, while exhibiting increased instability (-10). Profiles at 1300 and 2300 GMT for southwestern Georgia (Fig. 20) illustrate the changing conditions (#s in Fig. 17). With these profiles, the LI changes from -4 at 1300 GMT to -7 at 2300 GMT. In the boundary layer, surface heating warms the surface (850 mb level) approximately 7 °C (3.5 °C), although dewpoints change little. During the morning, VAS indicates that the

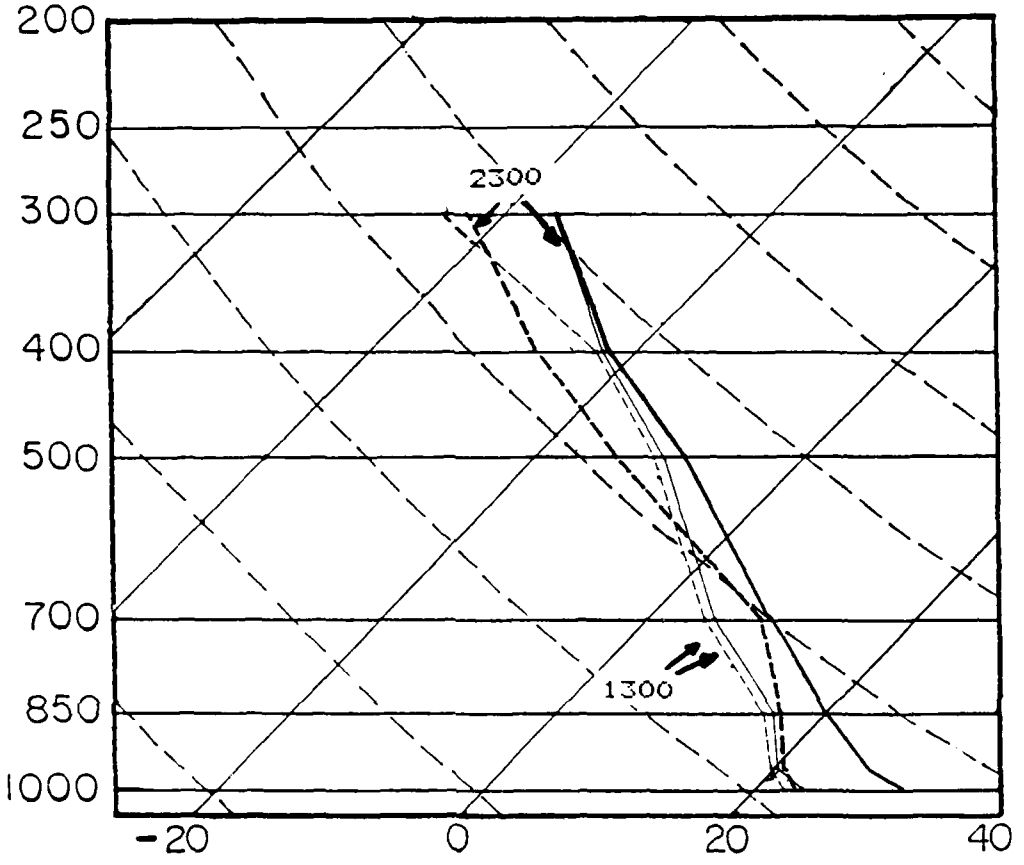


Fig. 20. [illegible] retrieved [illegible] # in Fig. 17.

atmosphere is relatively moist from the surface to near 400 mb, but later, with the exception of 700 mb, drying takes place at all levels. The increased temperatures between 850 and 500 mb cannot be explained, and are considered suspect. This is a specific example of the excessive diurnal variations produced by the simultaneous algorithm. One should recall, however, that only temperatures in the boundary layer and at 500 mb affect the LI.

In addition to the LI centers, several stability axes also provide useful information. At 1600 and 1700 GMT (Fig. 17), for example, there is an unstable axis (-6) across northern Arkansas and eastern Oklahoma. One to two hours later, satellite imagery (Fig. 6) reveals the development of a strong line of thunderstorms in the area that apparently was induced by an outflow boundary which propagated southward from a morning position over central Missouri. As a second example, there is an axis of relatively stable air at all five times from southern Louisiana to southern Mississippi. In this case, satellite imagery reveals the area to be largely convection free during the entire day. The 1300 and 2300 GMT VAS soundings (Fig. 21) for this location (*s in Fig. 17) indicate strong surface warming; however, dewpoints remain nearly constant. The relatively small amount of available moisture apparently is the reason for the lack of

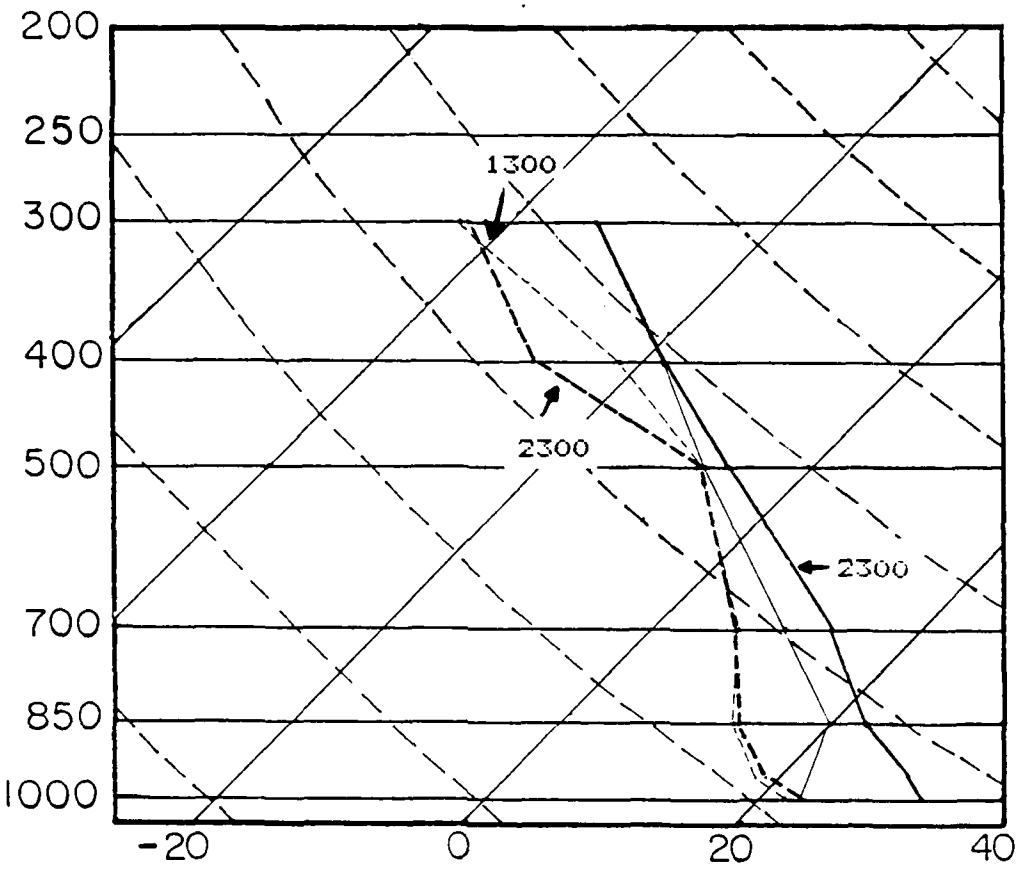


Fig. 21. VAS retrievals over southern Louisiana at 1300 (thin) and 2300 GMT (bold). Sounding locations are given by the symbol * in Fig. 17.

convective development. Once again, the 2-3°C increases in temperature above the boundary layer are suspect.

The final area of interest is major instability (-10) that develops at 2000 GMT over central Nebraska (Fig. 17). This first was thought to be a "false alarm", but radar charts for the upcoming evening (not shown) indicate that this area did experience strong convection, eventually forming a Mesoscale Convective Complex (MCC) over northeastern Kansas. Examination of 1300 and 2300 GMT profiles (Fig. 22) reveals marked warming near the surface (-12°C) during the day and an increase in low to mid level moisture. (Locations of the soundings are denoted by + s in Fig. 17.) The morning inversion is exaggerated by VAS, possibly due to a problem in "blending" the surface data into the "first guess" profile. At both times, however, the lapse rate becomes nearly dry adiabatic between 850 and 500 mb. Although Nebraska is preferentially cold at 500 mb (Fig. 10), there is little temperature change at these two sounding sites.

There is one notable area where VAS-derived LI (Fig. 17) was not a good indicator of convective activity. A band of showers and thunderstorms developed over extreme eastern Texas during the afternoon (Fig. 6), yet LI values remained relatively stable (0 to -2). Skies were cloud-free during the morning hours, providing abundant solar heating, and apparently there was sufficient small

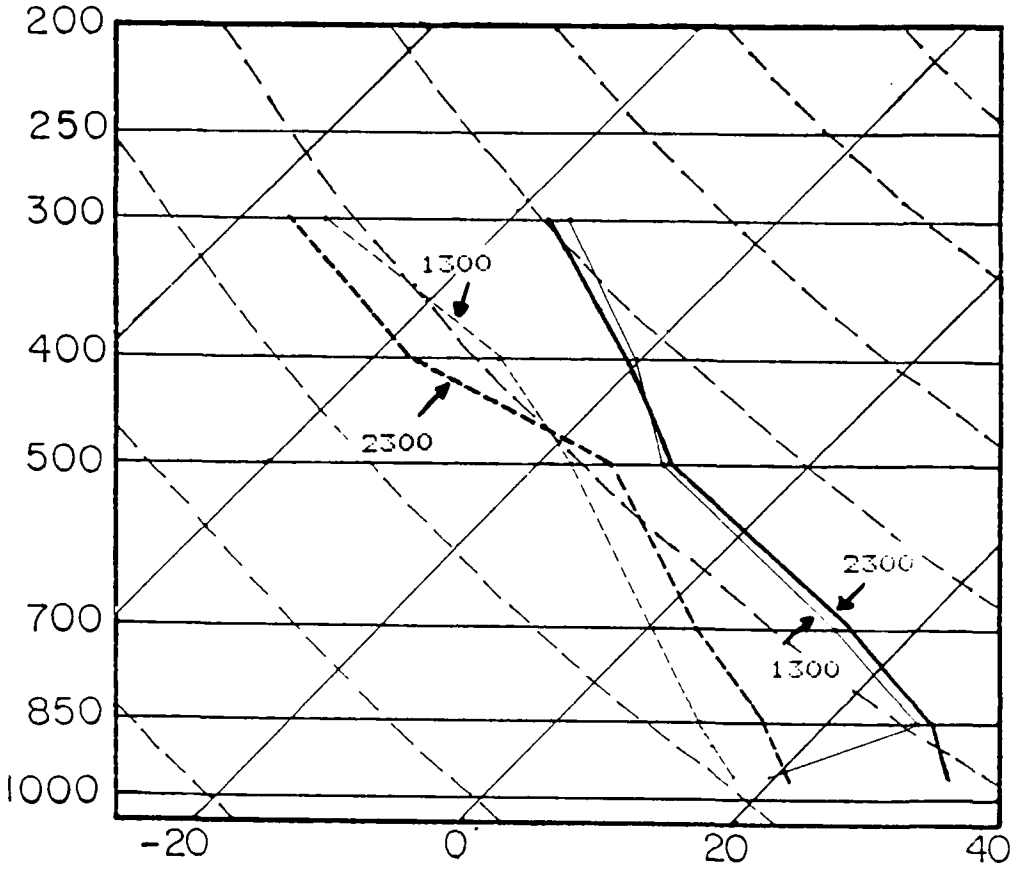


Fig 22. [illegible] retrievals over southeastern Nebraska [illegible] and [illegible] using [illegible] are [illegible] + in Fig. 17.

scale forcing to "trigger" even this marginally unstable air.

In summary, the VAS-derived LIs appear to be a valuable forecasting tool. That is, most of the relatively unstable areas coinsided with afternoon convection, while comparitively stable areas were storm free. Several larger scale stability features compared favorably with their RAOB-derived counterparts (Fig. 5), e.g., the major instability axis over the Mississippi River Valley and the development of strong instability in Nebraska. Of course, VAS was able to define these features at a finer scale. For example, several axes of instability and stability, e.g., the eastern Oklahoma to western Arkansas, and southern Louisiana locations would have "fallen through the cracks" of the national RAOB network. One must notice, however, that actual values of VAS-derived LI tend to be too negative, as observed by Anthony and Wade (1983) and others. Thus, as noted earlier, the forecaster should concentrate on the relative patterns and magnitudes of the features, and not their absolute values.

An important question about the enhanced resolution of VAS products still must be answered: Do VAS-derived values provide information that could not have been obtained from conventional surface data, i.e., is VAS merely duplicating results that could have been calculated from simple surface observations? To answer that question, LIs (Fig.

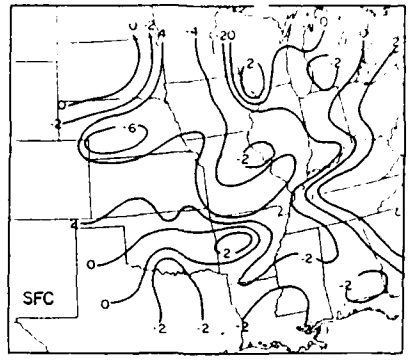


Fig. 23a. Change in surface-derived Lifted Index between 1600-2000 GMT.

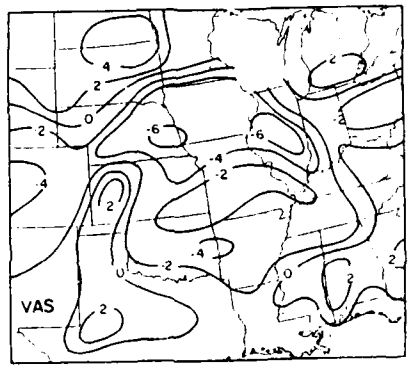


Fig. 23b. Change in VAS-derived Lifted Index between 1600-2000 GMT.

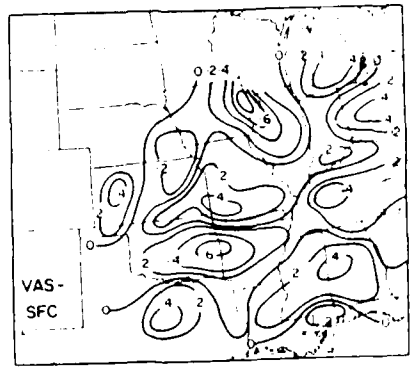


Fig. 23c. The difference between Figs. 23 a and b. Negative values indicate that VAS-derived LI become more negative with time than the surface-derived version.

23) were re-calculated using a technique similar to that employed by the NSSFC (Hales and Doswell, 1982). The scheme utilizes 500 mb temperatures together with conventional hourly reports of temperature and dewpoint. There was one difference between their method and that employed here, i.e., the current 500 mb temperature was held constant in time, whereas NSSFC routinely uses a 500 mb temperature forecast from one of the operational NMC models. Changes in LI based on the surface data variations then were calculated by subtracting the values at 1600 and 2000 GMT (Fig. 23a). A major assumption of the Hales and Doswell (1982) approach is that the surface data are representative of the entire 1 km boundary layer. While this probably is valid during the afternoon hours, it is not appropriate during the morning. Furthermore, after 2000 GMT, the surface data fields were heavily contaminated by thunderstorms, cooling the individual locations by precipitation and advection processes. Thus, only results for the 1600-2000 GMT time period are presented. Corresponding LI changes based solely on VAS retrievals are given in Fig. 23b; patterns at the individual times were given earlier in Fig. 17.

If VAS merely was duplicating the surface data, i.e., not providing independent information, the change fields from the two techniques (Fig. 23) would be similar. However, inspection of the figure reveals that this is not

the case. During the 1600-2000 GMT period, VAS indicates that northwestern Illinois, eastern Oklahoma, and eastern Nebraska were becoming more unstable by at least 4 units. Some increases in stability are noted in the vicinity of ongoing convection, e.g., southern Alabama and central Georgia. The surface-derived LIs (Fig. 23a) also display greater than -4 changes covering southeastern Nebraska, western Iowa, and western and southern Missouri; however, unlike the VAS product, stability increases occur over central Arkansas and eastern Oklahoma, and east of 85°W. To further compare the LI change fields, Fig. 23c shows differences between VAS- and surface-derived LI changes (i.e., differences between Figs. 23a, b). VAS-derived LIs are becoming more unstable than the surface-derived LIs over Iowa and Illinois as well as eastern Arkansas (larger negative values). On the other hand, when compared to results solely from the surface data, VAS indicated that central Texas, central Mississippi, southern Missouri, and western Kansas were becoming either slightly more stable or not as unstable as surface data suggested.

Based on Fig. 23, it is obvious that VAS does not simply duplicate the LI variations due to surface data fluctuations. Indeed, there were several large contrasts in the patterns of LI changes. Therefore, VAS is supplying the forecaster with information above the surface that is important in producing stability variations. Using the

satellite imagery as a standard, it appears that the VAS-derived LI changes are superior to those created solely from surface data. That is, areas that were becoming more unstable than indicated by surface data often experienced convection (Fig. 6), e.g., eastern Oklahoma, central Illinois, and central Tennessee. Conversely, areas where VAS indicated more of an increase in stability often were free of storms, e.g., southwestern Missouri, and Louisiana, Mississippi, and western Alabama.

A second question then arises: What information provided by VAS caused the resulting LI changes to be superior? The two possibilities are more realistic information about 500 mb temperatures, i.e., not the constant values assumed in Fig. 23, or improved low-level moisture depictions. Based on the sounding evaluations presented in Chapter 6, along with analyses of VAS-derived mid-level temperature variability (not shown), it appears that the latter is the significant contributor. Specifically, VAS's ability to describe moisture fields both horizontally (Fig. 9) and vertically apparently is the reason for its superior LI patterns. More importantly, Funk (1985) performed a similar investigation on LIs generated from the physical (Smith, 1983) algorithm but found that those versions did not provide much useful information over conventional surface data. Thus, it is encouraging that the new simultaneous profiles are an

improvement.

To summarize the LI findings, their improved resolution allows forecasters to concentrate on specific areas instead of larger regions. Although absolute values often did not compare closely with RAOB-derived versions, the large scale patterns were similar, and several smaller-scale features not apparent in the RAOB fields could be related to the presence or absence of storm activity. Finally, as just discussed, VAS appears to give the forecaster more than just a copy of surface induced LI variability; instead, it complements those data.

b. K Index

The "K Index" is a common parameter for forecasting summertime airmass convection and is given by

$$KI = (T_{850}-T_{500}) + DP_{850} - (T_{700}-DP_{700}), \qquad (11)$$

where T represents temperature, DP represents dewpoint, and the subscripts indicate the level of the measured data. The KI was designed to estimate thunderstorm potential on the merits of thermodynamics alone. Thus, there is not the requirement for dynamic lifting that is implicit with the LI. In fact, the KI does not perform as well as the LI when dynamic forcing is present. The KI is

a logical choice for the forecaster of summertime convection since large scale forcing is comparitively weak.

When radiosonde data are the input, typical summertime KI values range from 20 to 50, where 20 represents a 20-40% chance of a thunderstorm, and 50 indicates a 100% thunderstorm probability, along with a high likelihood of a severe weather event (Miller, 1972). Satellite derived KIs exhibit the same exaggerated values as the LIs, i.e., magnitudes tend to be too large. For example, KIs for the current case range from 30 to 65. No attempt was made to correlate these versions with the sonde-derived variety; instead, only relative strengths and patterns were examined.

A variation of the KI is the so-called "modified" K Index (Charba, 1979) in which surface dewpoint and temperature are averaged together with the 850 mb values. As one might expect, this procedure increases index values due to the higher averaged temperatures. Both versions of the index were calculated for the 21 July case. Since the modified variety consistently outperformed the original type, only the modified KIs (Fig. 24) will be shown.

At 1300 GMT, the KI analysis (Fig. 24) has maxima (instability) over eastern Missouri (51), northern Mississippi (50), and northwestern Georgia (50). During the morning hours, the maximum over Missouri appears to

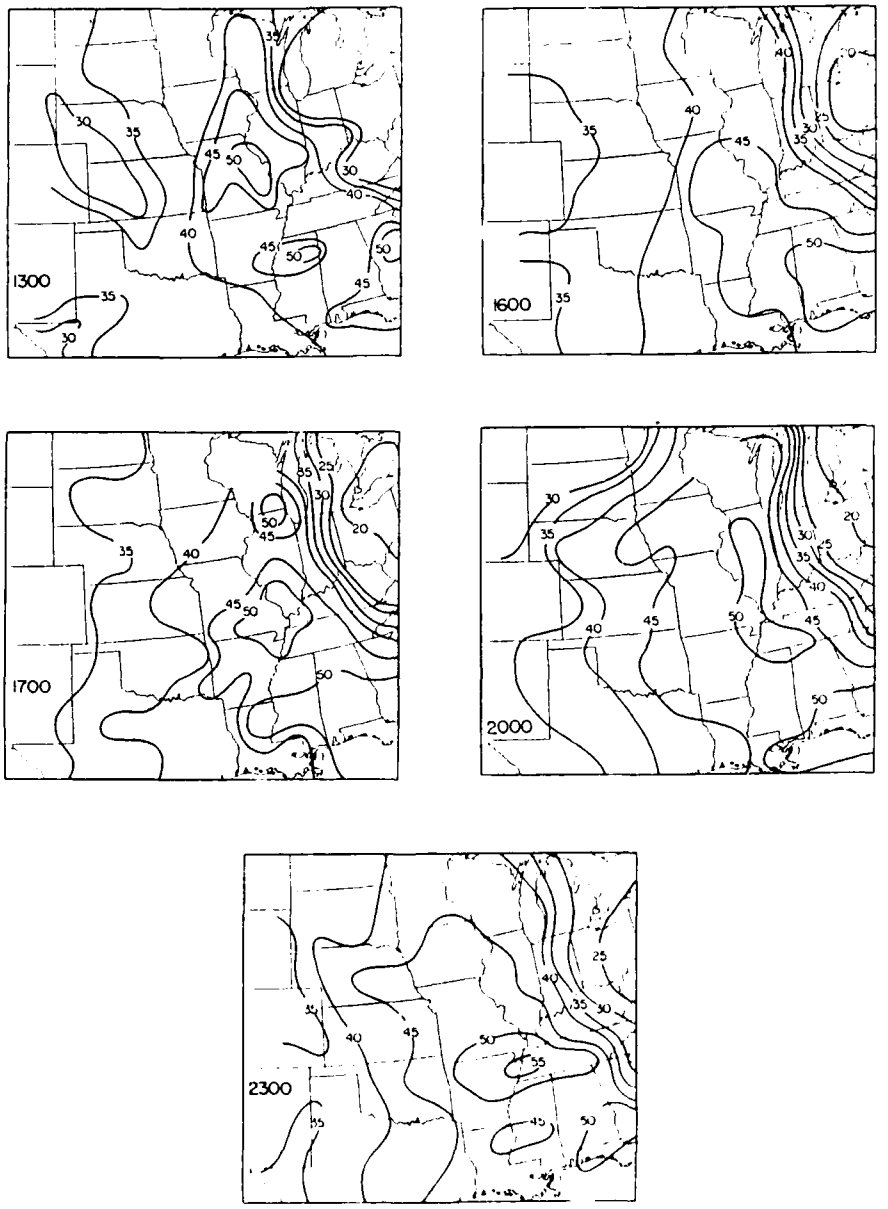


Fig. 24. VAS-derived K Index at the five observation times.

drift slightly to the east, generally maintaining its strength through 1700 GMT. The maximum over Mississippi loses intensity and becomes less well defined, while the maximum originally over Georgia moves toward the southwest with little change in intensity. An additional maximum develops over southern Wisconsin at 1600 GMT (near 45) and increases in strength by 1700 GMT (51).

During the afternoon, there is a north-south axis of instability along the Mississippi River Valley at 2000 GMT; however, this changes to an east-west alignment over Arkansas and Tennessee at 2300 GMT when values are greatest (55). Overall, the axis of instability moves little during the day although the individual maxima show some translation. The 2000 GMT analysis appears to have the best agreement with convection indicated by the satellite imagery (Fig. 6). On the other hand, this index also fails in predicting the convection over eastern Texas that was mentioned earlier.

KI patterns at 1300 GMT (Fig. 24) closely resemble the corresponding LI analysis (Fig. 17). Although movements of the individual KI maxima through the day are similar to those of the LI representation, the KI fields appear to lose definition in the afternoon. Furthermore, they do not develop the maximum over Nebraska. Thus, KI patterns at 2000 GMT do not agree as well with VAS-derived LI (Fig. 17), and, in general, they do not appear to give as good a

representation of stability as the LI analyses. This conclusion for 21 July agrees with that of Kitzmiller (1986) who found the KI providing less information than the LI during the afternoon.

c. Total Totals Index

The Total Totals Index (TT) is commonly used by military meteorologists. It is quick and easy to calculate, requiring information from only two levels. The TT is given by

$$TT = (T_{850} - 2T_{500}) + DP_{850}. \quad (12)$$

Radiosonde-derived values of TT normally range from 25 to 50, where a value greater than 40 indicates the possibility of a severe weather event. Again, VAS-derived versions usually are larger, ranging from 30 to 65. This index also can be modified by including surface data (Charba, 1979). Since the modified TT gave better results than the original version (as observed with the KI), only the former is displayed here.

At 1300 GMT (Fig. 25), there is a broad north-south area of instability stretching from Minnesota to the Gulf of Mexico. By 1600 GMT, an axis of greater instability develops over central South Dakota and Nebraska in

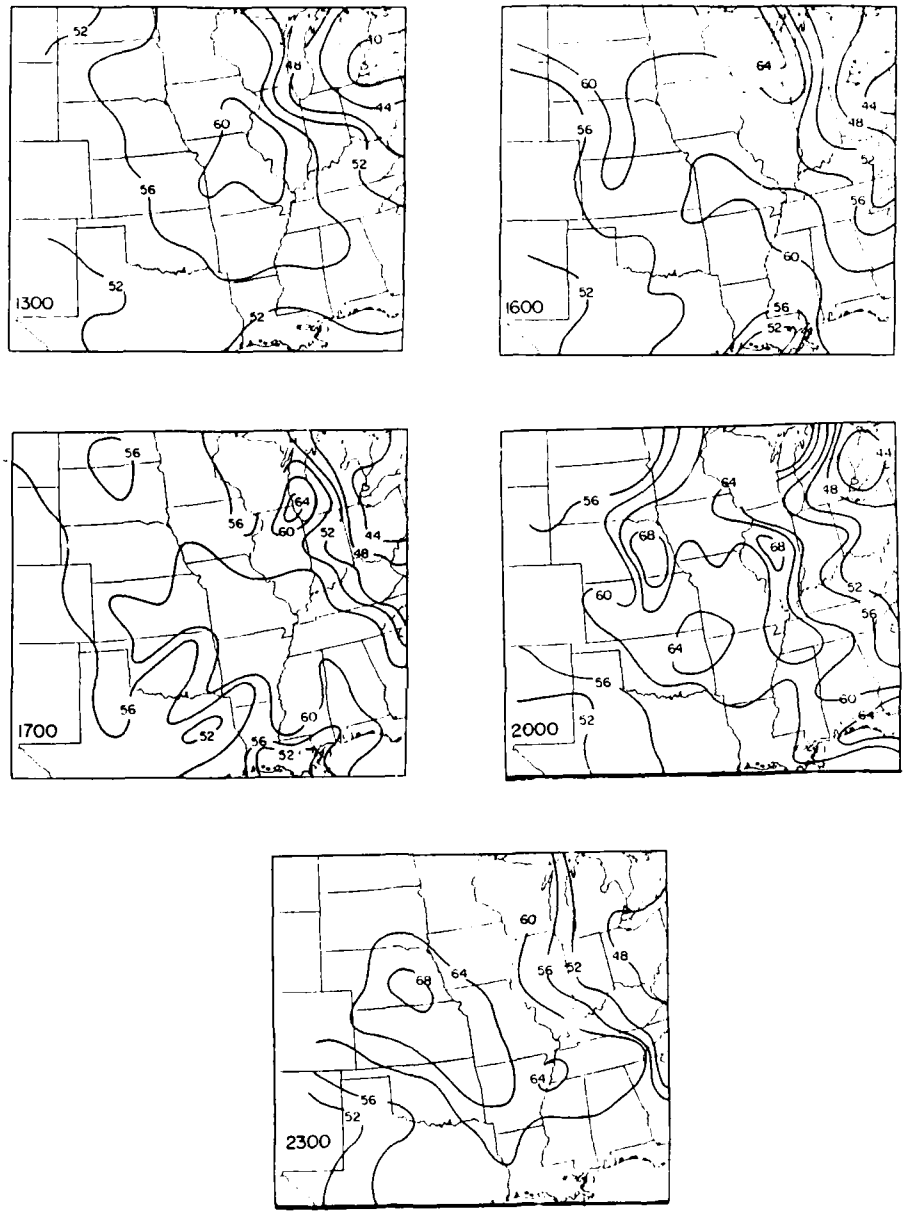


Fig. 25. VAS-derived Total Totals Index at the five observation times.

response to the VAS-analyzed 500 mb cold trough (Fig. 10). At 2000 GMT, a north-south axis of instability stretches from northern Illinois to western Tennessee, with a maximum of 68 over central Illinois. Another area of major instability (68) covers eastern Nebraska, while two others (64) are located over eastern Oklahoma and northwestern Florida. At 2300 GMT, the instability maximum over Nebraska becomes the dominant feature.

The TT analyses (Fig. 25) are similar to those of KI (Fig. 24) and LI (Fig. 17) over the Midwest and Southeast. Also, like the LI analyses, but unlike the kI, there is a strong instability region near Nebraska. Kitzmiller (1986) noted that the TT index did not perform as well as the LI; however, there is no clear distinction on 21 July.

## 8. Integrated parameters

The previous chapters have demonstrated that VAS can reasonably describe horizontal fields of temperature and dewpoint. However, since weighting functions of the sensor's spectral channels are so broad (Fig. 1), vertical resolution is poor. Several authors, e.g., Mostek *et al.* (1986), Zehr (1985), have suggested using parameters based on data from deep atmospheric layers rather than from discrete levels. Therefore, this chapter evaluates a variety of parameters and indexes which use the concept of layer integration. Personal communication with Dr. James Purdom of the National Environmental Satellite Data Information Service (NESDIS) was the impetus for this aspect of the research. Dr. Purdom kindly provided a program to calculate various parameters, and it was modified by the author to derive several additional variables. The investigated parameters include:

1. Mean mixing ratio in lowest kilometer,
2. Negative energy from surface to LCL,
3. Pressure of LCL,
4. Height of wet-bulb zero,
5. Negative energy from LCL to Level of Free Convection

(LFC),

6. Heating energy (HE) required for surface to reach Convective Temperature ($T_c$),

7. Total Negative Energy (NE),

8. Total Positive Buoyant Energy (PBE),

9. Total Positive Energy if surface temperature equals $T_c$,

10. Maximum Vertical Velocity, and

11. Precipitable Water (PW).

Zehr (1985) described positive buoyant energy as Convective Available Potential Energy (CAPE), which is the vertically integrated temperature difference between the environment and a warmer, buoyant parcel which has been adiabatically lifted to its LFC. This formulation does not include entrainment, and does not require a specific the lifting mechanism. On the other hand, it represents energy required to raise the parcel

Given a standard VAS-derived temperature and dewpoint, the above listed parameters calculated (Fig. 26). The mean numerical average of all values above the surface. Parameters required to lift the parcel represented by areas its pressure are determined LI calculations

AD-A186 158 ASSESSMENT OF VAS-DERIVED PRODUCTS CREATED BY A SIMULTANEOUS ALGORITHM ON.. (U) AIR FORCE INST OF TECH WRIGHT-PATTERSON AFB OH M J ANDREWS 1987 2/2

UNCLASSIFIED AFIT/CI/NR-87-104T F/G 4/2 NL

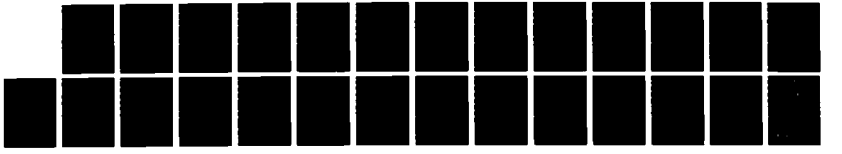

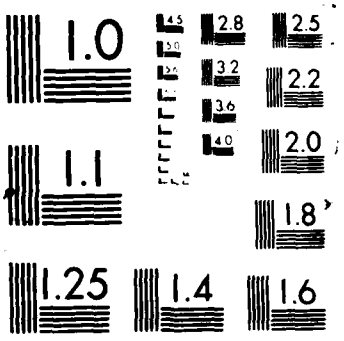
1.0
1.1
1.25
1.4
1.6
1.8
2.0
2.2
2.5
2.8
3.2
3.6
4.0

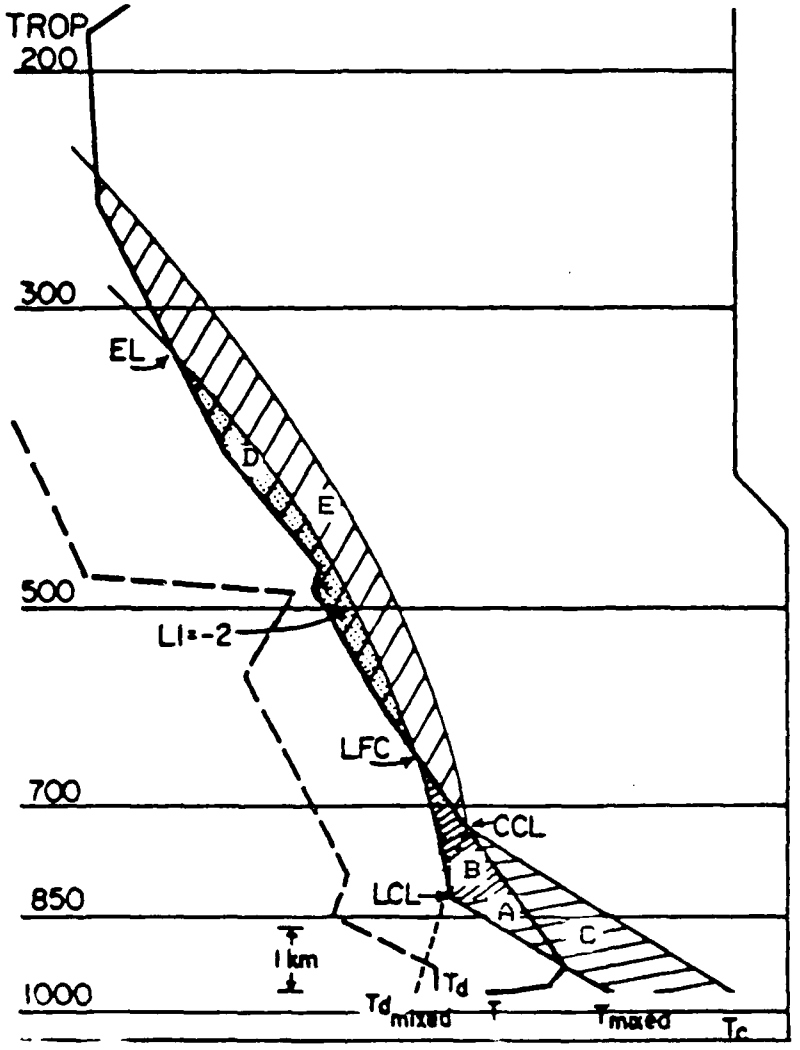


Fig. 26. Skew T-log P diagram illustrating bulk thermodynamic parameters computed from VAS retrievals (after Zehr, 1985).
Area A represents negative area from surface to LCL.
Area B represents negative area from LCL LFC.
Area C represents heating energy required for surface temperature to reach $T_c$.
Area D represents positive buoyant energy.
Area E represents available positive buoyant energy if surface reaches $T_c$.

wet-bulb zero is self explanatory. The heating energy required to raise the surface temperature to its convective value is represented by area C, while the total negative energy is merely the sum of parameters #2 and #5. Parameters #8 (area D) and #9 (area E) are energies that would be available to a parcel after having reached its LFC from either the original surface temperature (due to forced lifting), or from its convective temperature, respectively. The maximum vertical velocity is obtained from simple parcel considerations. Finally, precipitable water is integrated water vapor content throughout the depth of the sounding.

The eleven parameters were calculated at 1300, 1600, 1700, 2000, and 2300 GMT. Although each provided reasonable fields, several stood out from the others. Specifically, positive buoyant energy, total negative energy, heating energy required to reach surface convective temperature, and precipitable water analyses appeared to provide the most useful information. As a result, they will be described in the following pages.

a. Positive buoyant energy

Fig. 27 displays PBE for the five retrieval times. Patterns and evolutions of these analyses are consistent with those of the LIs (Fig. 17). For example, at 1300 GMT, major energy centers are located over eastern Missouri,

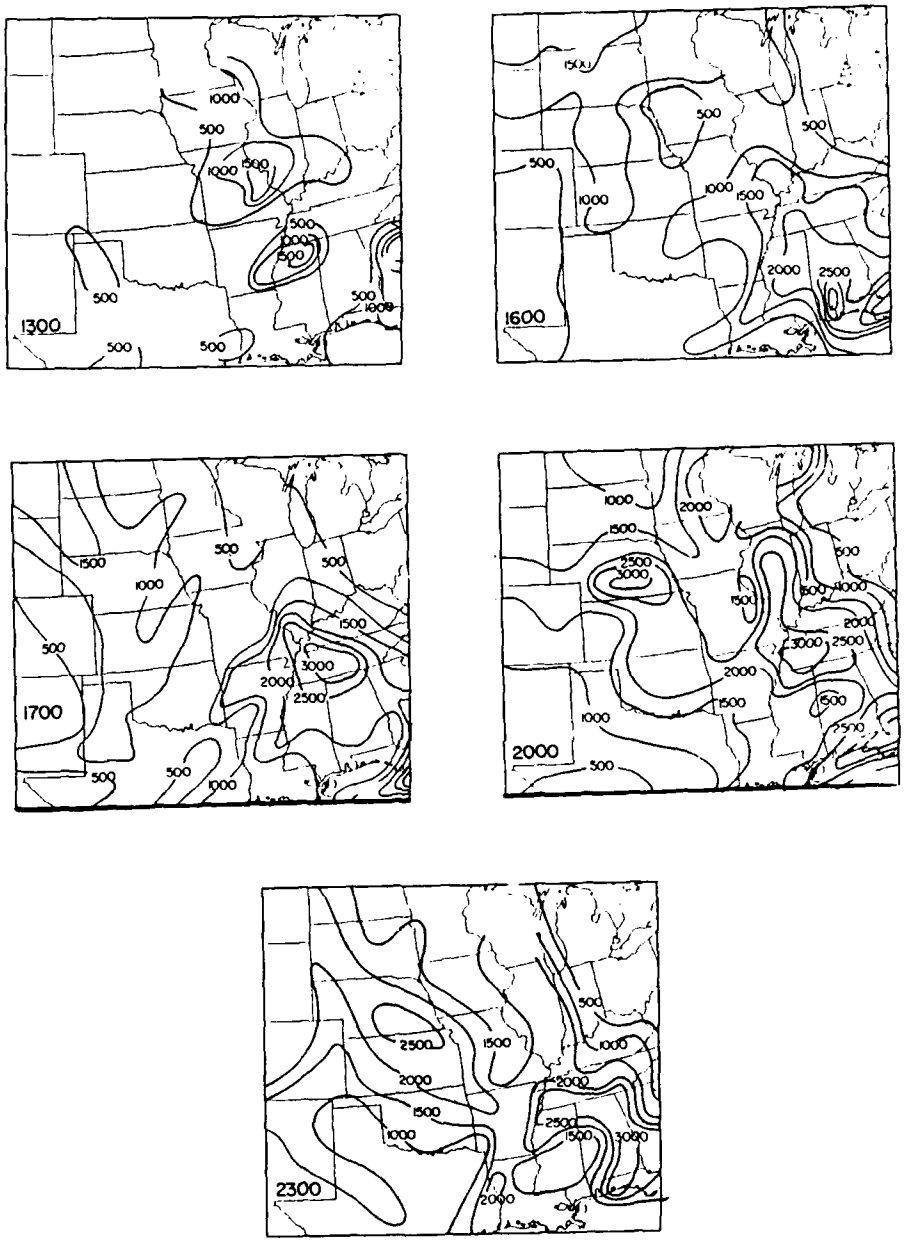


Fig. 27. VAS-derived total Positive Buoyant Energy (PBE) at the five observation times. Values are J/kg.

northern Mississippi, and northern Georgia. During the day, PBE increases greatly (~3500 J/kg) over southern Alabama, southern Georgia, and northern Florida, while another maximum (>3000 J/kg) develops over west central Tennessee. Satellite imagery (Fig. 6) shows the Southeastern maxima agreeing well with ongoing convection; yet the Tennessee area still is relatively convection free. Convection does take place shortly thereafter.

An axis of maximum PBE extends from western South Dakota to central Nebraska at 1700 GMT, and by 2000 GMT it becomes a strong, well defined center (3000 J/kg). This is similar to that of the LI analyses (Fig. 17); however, as discussed earlier, no convection takes place until much later. Elsewhere, a minimum (< 1500 J/kg) develops over eastern Missouri, persisting through the late afternoon. Finally, relatively large values over eastern Oklahoma at 1600 and 1700 GMT and the minimum axis covering portions of central Louisiana, Mississippi, and Alabama at several times both agree with LI features.

Zehr (1985) noted that values of PBE exceeded 750 J/kg in areas of ongoing convection and that PBE maxima outlined preferred areas of convection. In the current case however, areas > 750 J/kg did not necessarily have concurrent convection, e.g., most of the Plains States had afternoon values greater than 1500 J/Kg, yet skies remained clear. Obviously, other factors, e.g., inadequate

moisture or a lack of forcing are preventing that energy from being realized. Concerning similarities between PBE and LI, this is expected since procedures for obtaining their values are closely related. Specifically, the LI is the difference between the lifted parcel temperature and the environmental value at 500 mb, while PBE is the integrated temperature difference between the raised parcel and the environmental sounding at all levels above the LFC (where the parcel is warmer). Furthermore, since VAS data only are available at the mandatory levels, the 500 mb value has a major impact on the overall profile.

b. Total negative energy

Total negative energy describes inhibition to convective activity. The negative region acts as a hurdle which the sub-cloud parcel must overcome by heating or lifting before even large PBE can be utilized. Fields of NE are presented in Fig. 28. Whereas PBE (Fig. 27) and LI (Fig. 17) analyses compared closely, the NE patterns are much different. In this case, maximum NE represents a stronger "cap", i.e., a greater amount of lifting or heating is required for a parcel to reach its LFC.

At 1300 GMT (Fig. 28), an axis of minimum NE (< 200 J/kg) extends from southern Minnesota to eastern Missouri, then eastward to central Kentucky, and finally southward

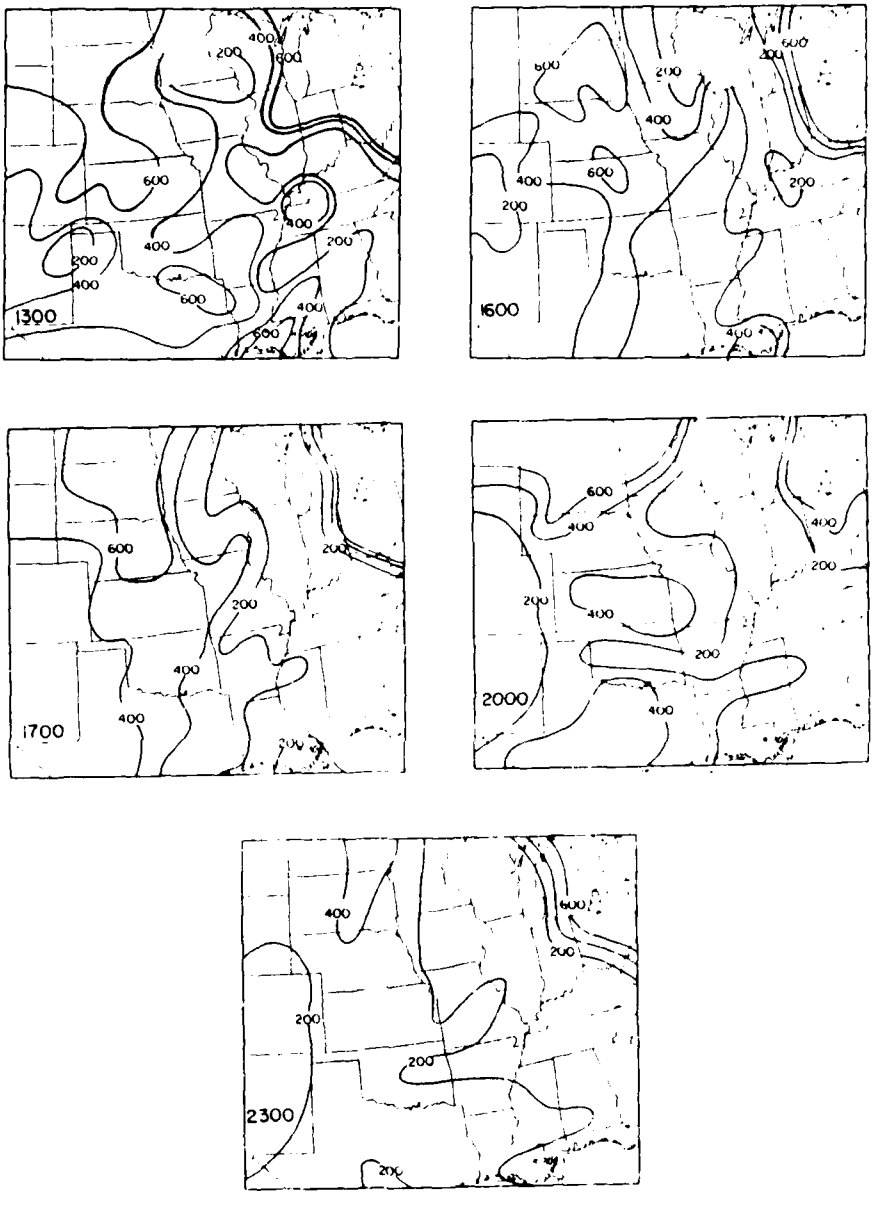


Fig. 28. VAS-derived total Negative Buoyant Energy (NE) at the five observation times. Values are J/kg.

to northern Florida. This area of minimum suppression generally is in the same location as the maximum axes of both LI (Fig. 17) and PBE (Fig. 27). There are two relative maxima of NE--over northeastern Texas and Arkansas (500 J/kg), and stretching from western South Dakota to central Kansas. The northeastern corner of the domain has NE exceeding 1000 J/kg, thereby indicating that convection is very unlikely.

By 1700 GMT (Fig. 28), the axis of minimum NE has shifted slightly eastward, with values < 100 J/kg occurring over much of the Southeast. Minor minimum axes cross central Iowa (250 J/kg) and southern Missouri (150 J/kg). The maximum axis over Texas maintains its position but weakens (400 J/kg), while the maximum over Nebraska shifts slightly eastward at nearly constant strength. The 2000 GMT analysis shows that the major minimum axis changes little, yet the smaller ones continue to grow. The first now covers most of Iowa, while the second extends westward from Arkansas to western Oklahoma. The maximum over Nebraska appears to split, with one region over eastern Kansas (450 J/kg) and the second over South Dakota (600 J/kg). Finally, between 2000-2300 GMT, there is a significant change in the maximum over Nebraska and Kansas where values decrease 40 - 50% over those three hours earlier. This trend, if continued, would account for the delay in convective activity over Kansas which began near

0600 GMT.

Overall, there is a consistent relation between NE (Fig. 28) and thunderstorm activity (Fig. 6). That is, NE maxima correspond to little convection, regardless of PBE strength, and rarely does deep convection occur with NE greater than 250 J/kg. This alone appears to be a valuable forecasting tool.

The use of energy parameters for predicting convective activity is not new. Normand (1938) categorized atmospheric soundings into three classes: no latent instability, psuedo-latent instability, and real latent instability. When PBE was zero, the sounding was said to have no latent instability. Furthermore, if PBE was greater than zero, but less than NE, the sounding had "psuedo-latent" instability. On the other hand, if the PBE exceeded NE, then the sounding had real latent instability. Thus, Normand (1938) attempted to combine NE and PBE into one index which would predict convection; however, his theories were not widely accepted. Others felt that combinations were not relevant, since even small negative energy can prevent a large positive value from producing storms. On the other hand, the ability to describe these parameters at the small scale (spatially and temporally), and perhaps more importantly, their changes, demands renewed investigation of this concept.

c. Heating to reach convective temperature

There are several mechanisms which allow parcels to overcome their negative energy barriers, e.g., frontal lifting, orographic lifting, and heating. Fig. 29 depicts the heating required to raise the surface temperature to the convective temperature, i.e., the amount of heat energy which would raise the parcel's LCL to its LFC. Like the NE analyses (Fig. 28), large HE indicates that a greater amount of heating is nessesary for convection, therefore, convection based on heating alone would not be as likely. Conversely, minimum HE indicates a preferred area for heating induced convection.

HE patterns at 1300 GMT (Fig. 29) contain a minimum axis (200 J/kg) stretching from Indiana southward to northern Florida, while a maximum covers northeastern Texas (700 J/kg). The Northeast is a region of large HE. HE decreases over the entire area by 1600 GMT (Fig. 29), and this is expected due to diurnal heating. Although the minimum axis does not appear to change position, a maximum axis moves out of the Dakotas into Nebraska and Iowa. By 1700 GMT, the north-south minimum remains quasi-stationary; however, a tongue of minimum values develops across northern Arkansas and southern Missouri (150 J/kg). This particular axis seems to match the outflow boundary from the morning convection over central Missouri that was suggested by satellite imagery (Fig. 6).

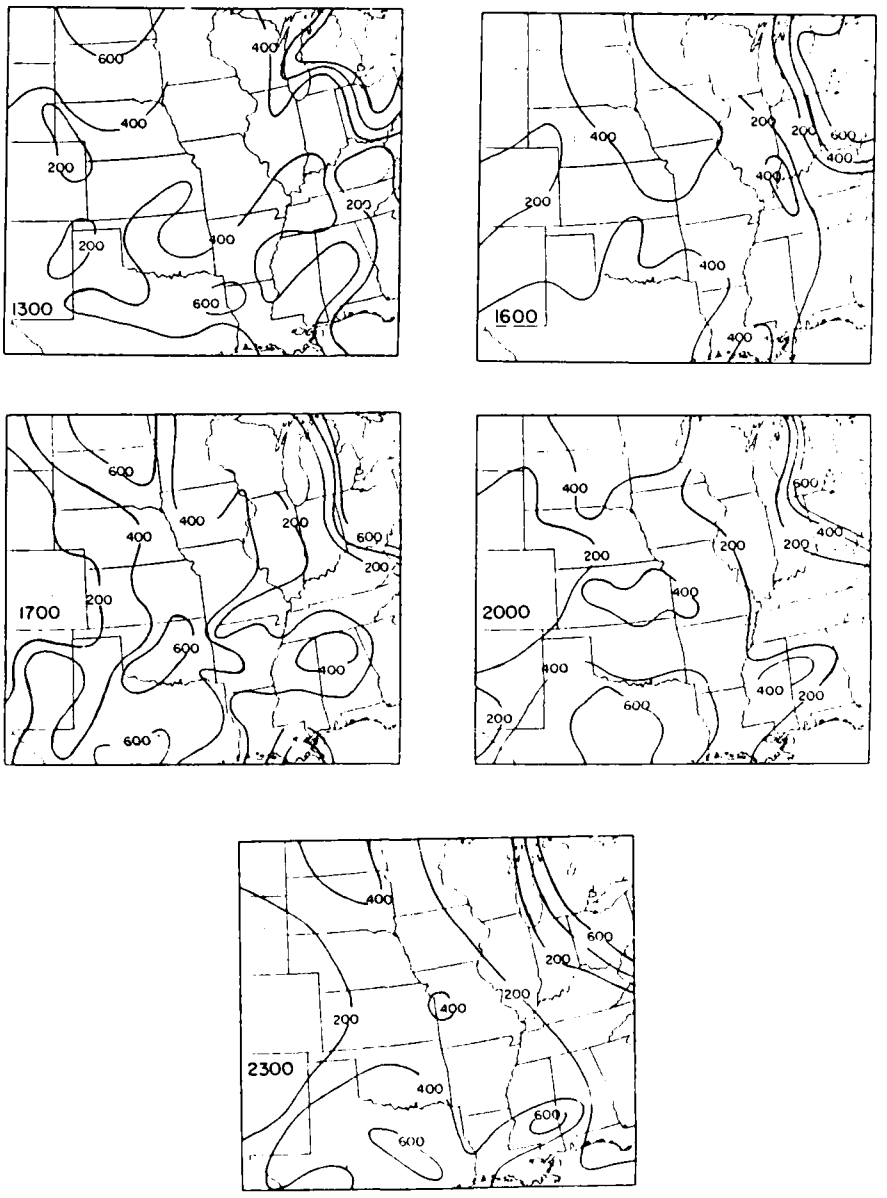


Fig. 29. VAS-derived Heat Energy (HE) required for surface to reach the convective temperature. Values are J/kg.

The maximum axis appears to strengthen, with a center developing over Oklahoma (650 J/kg).

During the late afternoon hours (2000 and 2300 GMT, Fig. 29), the major minimum axis continues to cover the Southeast; however, the northern portion appears to move slightly westward into northern Illinois. Most of the maxima show only minor fluctuations; however, values over Nebraska fall 50%, comparable to results of NE (Fig. 28).

There does not appear to be a well defined "critical" HE value which delineates the presence or absence of convection. For example, thunderstorms form over Arkansas where HE reaches 375 J/kg (recall the outflow boundaries in Fig. 6), and they develop over eastern Texas where HE exceeds 600 J/kg. This may suggest that HE predicts areas of preferred convective development, but will not indicate areas where convective growth is inhibited.

d. Precipitable water

Water vapor content is an ingredient to many of the stability parameters described here and in Chapter 7, and it is valuable to consider it separately. Precipitable water represents the integrated vapor of an atmospheric column. Fig. 30 displays values for the total surface to 300 mb layer. Values range from 2.5 to 6.5 cm, which is typical of RAOB-derived values during summertime. Patterns

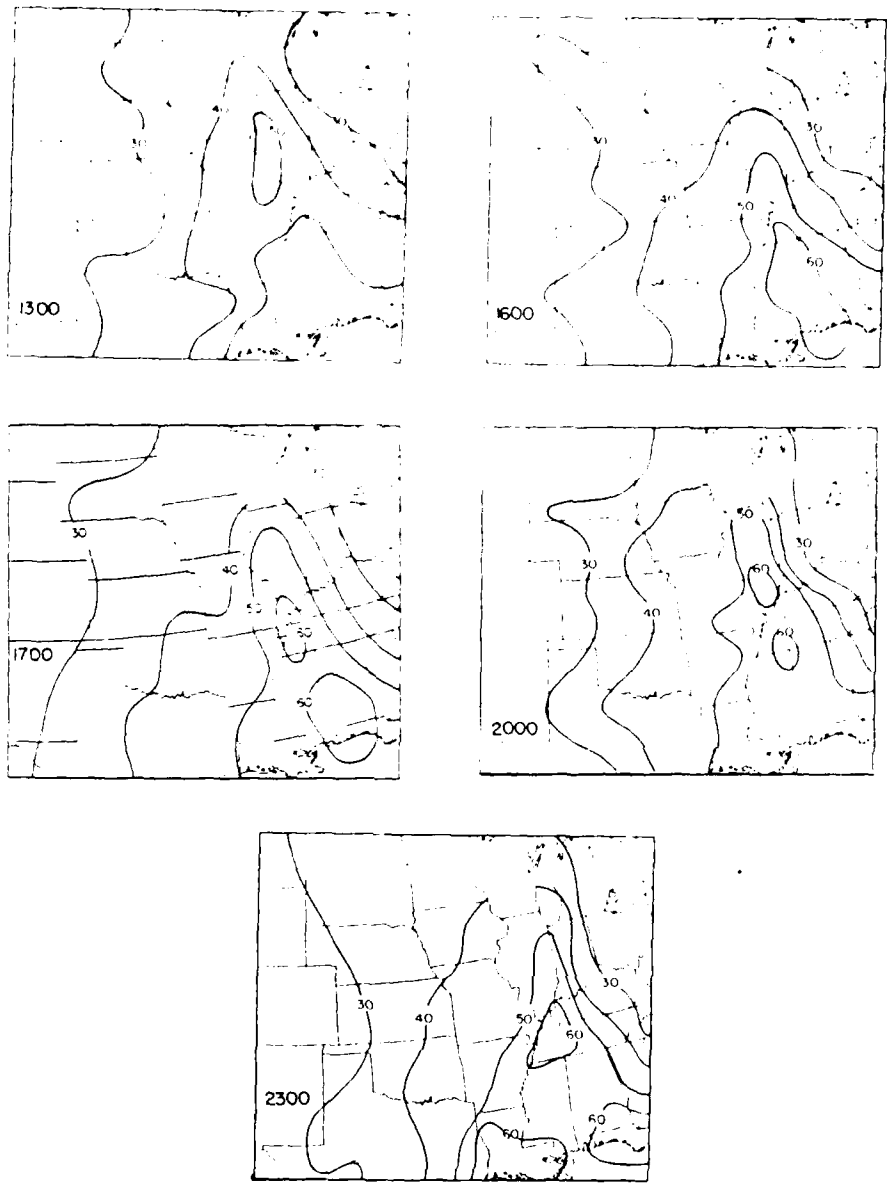


Fig. 30. VAS-derived precipitable water for the surface to 300 mb layer at the five observation times. The value 40 represents 4.0 cm.

and evolutions are similar to those of 850 mb dewpoint (Fig. 9). An axis of maximum PW (> 4.0 cm) extends from southern Wisconsin to the Gulf Coast at 1300 GMT (Fig. 30), shifting slowly to the east with time. Values reaching 6.0 cm develop over Mississippi at 1600 GMT and move north during the afternoon, eventually covering southern Illinois where the intense convection develops. Values are less than 2.0 cm over the Northeast and the eastern Rockies, the latter mostly due to the reduced thickness of the column.

To explore vertical characteristics of the moisture, PW was calculated over three component columns: Surface - 700 mb, 700 - 500 mb, and 500 - 300 mb. Results for 2000 GMT are shown in Fig. 31. As one might expect, most of the moisture is found in the lowest layer. The middle layer appears to contain about 25% of the total amount while the upper layer contains less than 5 %. There appears to be a slight eastward shift in the PW axis with altitude, with the upper level position extending approximately 100 km east of the low level axis over Illinois. It is possible that cirrus blowoff from the afternoon convection over western Illinois already had advected to the east, contributing to the vertical slant of the moisture axis. The low levels over eastern Missouri contain a minimum of vapor due to the outflow boundary; however, no major areas of mid level dryness are evident in PW or in the

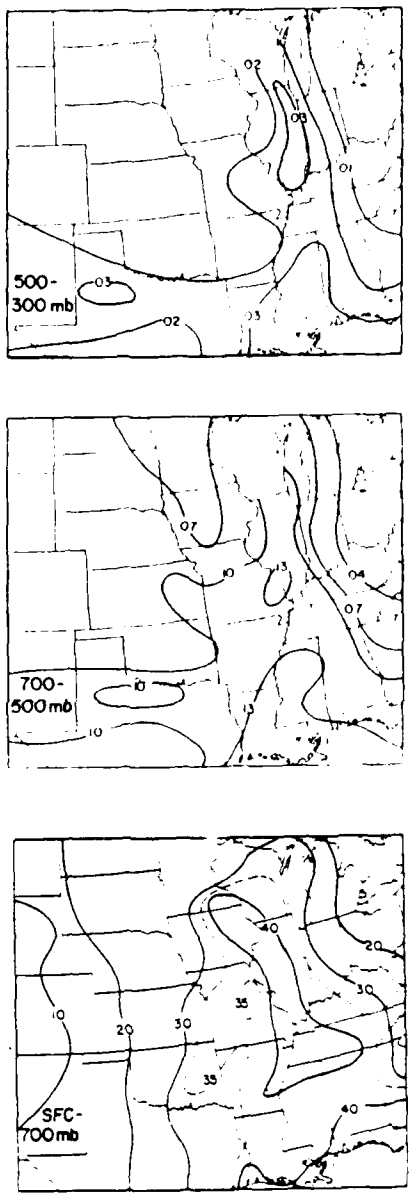


Fig. 31. VAS-derived precipitable water for three layers--surface-700 mb, 700-500 mb, and 500-300 mb. The value 13 represents 1.3 cm.

individual soundings (Figs. 18-22). Consequently, convective instability is not a factor in producing the storm outbreak. Overall, PW fields differ only slightly from those of 850 mb dewpoint, and they provide little additional information.

## 9. Summary and conclusions

A "new" physical retrieval algorithm which converts atmospheric radiances measured from a space platform into vertical profiles of temperature and moisture has been evaluated for a "typical" summertime day in July 1982. The area of interest was the midwestern United States where data coverage was excellent. Sounding products were available at intervals of 2-3 h for a total of 5 times. After a brief review of the two different retrieval algorithms, RMS errors for the new simultaneous scheme were compared to those from an earlier version, using radiosonde reports as a standard. VAS-derived fields of temperature and dewpoint were evaluated for both spatial and temporal continuity. Next, numerous stability indices calculated from the satellite-derived profiles were compared to visible satellite imagery. Their ability to define small scale stability features and information not obtainable from conventional sources was examined extensively.

Overall, soundings from the new retrieval algorithm were favorable; however, there also were some limitations. Compared to results for the older version, there was marked improvement in moisture analyses which exhibited

good continuity from one time to another. On the other hand, while temperature patterns corresponded to observed RAOB analyses, mean errors were somewhat greater although RMS errors changed little. The newer VAS-derived soundings still exhibited errors considerably greater than their RAOB counterparts, and unrealistic diurnal trends continued to occur. The theoretical aspects of how changes in the algorithm have altered its overall performance were not the subject of this research. However, it appears that the more realistic "first guess" water vapor profile is a significant contributor to the noted improvement in moisture analysis. The problem of biased radiances from the radiometer underscores the need to consider retrieval variations, and not actual magnitudes.

Non-integrated and integrated stability indices were calculated because of the improvement in moisture definition. The Lifted Index appears to be a promising VAS-derived convection predictor. LI analyses maintained reasonable continuity, and provided useful information about several locations which was not available from either RAOB or surface observations. In many cases, the VAS-derived LI patterns were superior to those from RAOBs; however, the satellite's values were considerably more negative. Apparently, better low-level moisture analyses were a major contributor to this success.

Total Totals and K Indexes appeared to give a

convection forecaster reasonable information, but patterns were not as well defined as those of LI. Also, most features in the KI and TT analyses were present in the LI fields. In other words, KI and TT often detected the same major stability centers as did the LI; however, the LI analyses better defined smaller scale features, e.g., minor axes of stablility.

Eleven integrated parameters were calculated; several provided valuable information. Specifically, fields of positive and negative buoyant energy appeared to isolate areas which later contained strong convection, or on the other hand, remained convection free. As expected, there generally was good agreement with the non-integrated LIs. Heating energy required to raise the surface to its convective temperature provided some insight into the "timing" (onset) of convection; however, these fields generally were similiar to those of NE. Finally, VAS precipitable water analyses closely matched low-level moisture fields depicted by VAS, and values were consistent with RAOB analyses.

It may seem that the author is overly optimistic about the performance of VAS-derived parameters. However, having spent several summers forecasting convection over the United States at AFGWC in conjunction with the NSSFC, it quickly became clear that in the absence of stronger springtime dynamics, a good summertime convective forecast

is difficult, at best. Thus, VAS's ability to provide reasonable information about atmospheric stability in a short time is a welcome advance. Obviously, based on the error characteristics discussed earlier, refinements in the sensors and retrieval process are needed. Specifically, RAOBs are superior in the vertical resolution of the atmospheric state, and they provide smaller RMS measurement errors. Thus, an underlying point is user beware. Nonetheless, because of the large improvement in moisture fields defined by the new algorithm, and VAS's ability to provide hemispheric values in near real time with a much greater temporal resolution, it is clear that satellite data are destined to become a major contributor to tomorrow's atmospheric prediction models. By understanding this valuable tool, improvements in today's forecasts can be expected.

## REFERENCES


Anthony, R.W. and G.S. Wade, 1983: VAS operational assessment findings for Spring 1982/83. Preprints, 13th Conf. Severe Local Storms, Tulsa, Amer. Met. Soc., J23-J28.

Charba, J.P., 1979: Two to six hour severe local storm probabilities: An operational forecasting system. Mon. Wea. Rev., 107, 268-282.

Chesters, D., L. W. Uccellini and W. Robinson, 1983: Low-level moisture images from the VISSR Atmospheric Sounder (VAS) "split-window" channels at 11 and 12 microns. J. Climate Appl. Met., 22, 725-743.

_____, T. H. Lee, A. Mostek, and D. A. Keyser, 1984: The accuracy of mesoscale temperature and dewpoint fields retrieved from VAS satellite and conventional surface data. Preprints, Conf. Satellite Met./Remote Sensing and Applications, Clearwater Beach, Amer. Met. Soc., 226-231.

Fuelberg, H.E., and P.J. Meyer, 1985: An analysis of mesoscale VAS retrievals using statistical structure functions. J. Climate Appl. Met., 25, 59-76.

_____, and T.W. Funk, 1987: Diagnosis of vertical motion

from VAS retrievals. Submitted to Mon. Wea. Rev.

Funk, T.W., 1985: Diagnosis of vertical motions from VAS retrievals during a convective outbreak. Master's thesis submitted to St. Louis University.

Gruber, A., and C.D. Watkins, 1982: Statistical assessment of the quality of TIROS-N and NOAA-6 satellite soundings. Mon. Wea. Rev., 110, 243-252.

Hales, J.E., Jr. and C.A. Doswell, III, 1982: High resolution diagnosis of instability using hourly surface lifted parcel temperatures. Preprints, 13th Conf. Severe Local Storms, San Antonio, Amer. Met. Soc., 172-175.

Jedlovec, G.J., 1985: An evaluation and comparison of vertical profile data from the VISSR Atmospheric Sounder (VAS). J. Atmos. Ocean. Tech., 2, 559-581.

Kitzmiller, D.H., 1986: An objective comparison of severe local storm predictors derived from VAS temperature and dew point profiles. Preprints, 2nd Conf. Sat. Met./Remote Sensing and Appl., Williamsburg, Amer. Met. Soc., 353-358.

Lee, T.H., D. Chesters, and A. Mostek, 1983: The impact of conventional surface data upon VAS regression retrievals in the lower troposphere. J. Climate Appl. Met., 22, 1853-1874.

Leftwich, P.W., Jr., 1985: Operational estimations of hail diameter from VAS-derived vertical sounding data.

Preprints, 2nd Conf. Met./Remote Sensing and Appl., Williamsburg, Amer. Met. Soc., 193-196.

Lenhard, R.W., 1970: Accuracy of radiosonde temperature and pressure-height determination. Bull. Amer. Met. Soc., 51, 842-846.

Menzel, W.P., W.L. Smith, and L.D. Herman, 1981: Visible infrared spin-scan radiometer atmospheric sounder radiometric calibration: An inflight evaluation from inter-comparisons with HIRS and radiosonde measurements. Appl. Opt., 20, 3641-3644.

Miller, R.C. 1972: Notes on analysis and severe-storm forecasting procedures of the Air Force Global Weather Central. Air Weather Service Tech. Rep 200. (Rev.), U.S. Air Force, 102 pp. [NTIS AD 744 042].

Mostek, A., L.W. Uccellini, R.A. Petersen, and D. Chesters, 1986: Assessment of VAS soundings in the analysis of a pre-convective environment. Mon. Wea. Rev., 114, 62-87.

Normand, C.W.B., 1938: On instability from water vapour. Quart. J. Royal Met. Soc., 64, 47-69.

Petersen, R.A., L.W. Uccellini, D. Chesters, and A. Mostek, 1982: The use of VAS satellite data in weather analysis, prediction, and diagnosis. National Wea. Digest, 8, 12-23.

_____, _____, A. Mostek, and D.A. Keyser, 1984: Delineating mid- and low-level water vapor patterns in

pre-convective environments using VAS moisture channels. Mon. Wea. Rev., 112, 2178-2198.

Phillips, N., L.M. McMillin, A. Gruber, and D.W. Wark, 1979: An evaluation of early operational temperature soundings from TIROS-N. Bull. Amer. Met. Soc., 16, 1188-1197.

Raymond, D., H. Corbin, M. Desbois, G. Szejwach, and P. Waldteufel, 1981: The dynamics of polar jet streams as depicted by the METEOSAT water vapor channel radiance field. Mon. Wea. Rev., 109, 2164-2176.

Rogers, E.B., V.V. Salomonson, and H.L. Kyle, 1976: Upper tropospheric dynamics as reflected in Nimbus 4 THIR 6.7 um data. J. Geophys. Res., 81, 5749-5758.

Smith, W.L., 1970: Iterative solution to the radiative transfer equation for the temperature and absorbing gas profile of an atmosphere. Appl. Opt., 9, 1993-1999.

_____, 1983: The retrieval of atmospheric profiles from VAS geostationary radiance observations. J. Atmos. Sci., 40, 2025-2035.

_____, H.M. Woolf, C.M. Hayden, D.Q. Wark, and L.M. McMillin, 1979: The TIROS-N operational vertical sounder. Bull. Amer. Met. Soc., 60, 1177-1187.

_____, and F.X. Zhou, 1982: Rapid extraction of layer relative humidity, geopotential thickness, and atmospheric stability from satellite sounding

radiometer data. Appl. Opt., 21, 924-928.

_____, V.E. Suomi, F.X. Zhou, and W.P. Menzel, 1982: Nowcasting applications of geostationary satellite atmospheric sounding data. Nowcasting, Ed. K.A. Browning, Academic Press, 123-135.

_____, and H. Woolf, 1984: Improved vertical soundings from an amalgamation of polar and geostationary radiance observations. Preprints, Conf. on Satellite Met./Remote Sensing and Appl., Clearwater Beach, Amer. Met. Soc., 45-48.

_____, and C.M. Hayden, 1986: The international TOVS processing package. Unpublished manuscript provided in personal communication.

Steranka, J., L.J. Allison, and V.V. Salomonson, 1973: Application of Nimbus 4 THIR 6.7um observation to regional and global moisture and wind field analyses. J. Appl. Met., 12, 386-395.

Stewart, T.R., C.M. Hayden, and W.L. Smith, 1985: A note on water vapor wind tracking using VAS data on McIDAS. Bull. Amer. Met. Soc., 66, 111-115.

Stewart, M.R., and H.E. Fuelberg, 1986: Relationships between 6.7 micrometer imagery and radiosonde-derived parameters. Preprints, 2nd Conf. Sat. Met./Remote Sensing and Appl., Williamsburg, Amer. Met. Soc., 67-72.

Wade, G.S., A.L. Siebers, and R.W. Anthony, 1985: An

examination of current atmospheric stability and moisture products retrieved from VAS measurements in real-time for the NSSFC. Preprints, 14th Conf. Severe Local Storms, Indianapolis, Amer. Met. Soc., 105-108.

Zehr, R.M., 1985: Analysis of mesoscale air masses with VAS retrievals. Preprints, 2nd Conf. Sat. Met/Remote Sensing and Appl., Williamsburg, Amer. Met. Soc., 347-352.

END

12-87

DTIC